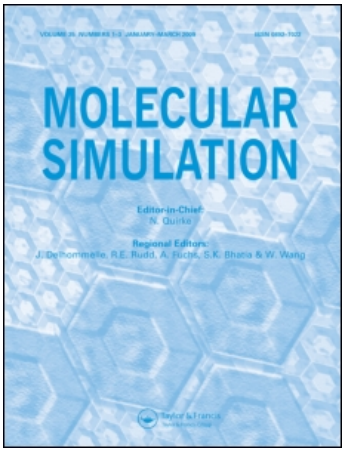

Molecular Simulation
Publication details, including instructions for authors and subscription information:
http://www.informaworld.com/smpp/title~content=t713644482

Interaction of alginate single-chain polyguluronate segments with mono- and divalent metal cations: a comparative molecular dynamics study

Lovorka Perić-Hassler[a]; Philippe H. Hünenberger[a]
[a] Laboratory of Physical Chemistry, ETH Zürich, Zürich, Switzerland

Online publication date: 15 October 2010

To cite this Article Perić-Hassler, Lovorka and Hünenberger, Philippe H.(2010) 'Interaction of alginate single-chain polyguluronate segments with mono- and divalent metal cations: a comparative molecular dynamics study', Molecular Simulation, 36: 10, 778 — 795
To link to this Article: DOI: 10.1080/08927021003752853
URL: http://dx.doi.org/10.1080/08927021003752853

Molecular Simulation
Vol. 36, No. 10, September 2010, 778–795

Taylor & Francis
Taylor & Francis Group

Interaction of alginate single-chain polyguluronate segments with mono- and divalent metal cations: a comparative molecular dynamics study

Lovorka Perić-Hassler and Philippe H. Hünenberger*

Laboratory of Physical Chemistry, ETH Zürich, CH-8093 Zürich, Switzerland

(*Received 19 November 2009; final version received 5 March 2010*)

The interaction of a set of monovalent (Na^+, K^+) and divalent (Mg^{2+}, Ca^{2+}) metal cations with single-chain polyguluronate (periodic chain based on a dodecameric repeat unit, 2_1-helical conformation) is investigated using explicit-solvent molecular dynamics simulations (at 300 K and 1 bar). A total of 14 (neutralising) combinations of the different ions are considered (single type of cation or simultaneous presence of two types of cation, either in the presence or absence of chloride anions). The main observations are: (1) the chain conformation and intramolecular hydrogen bonding is insensitive to the counter-ion environment; (2) the binding of the cations is essentially non-specific for all ions considered (counter-ion atmosphere confined within a cylinder of high ionic density, but no well-defined binding sites); (3) the density and tightness of the distributions of the different cations within the counter-ion atmosphere follow the approximate sequence $Ca^{2+} > Mg^{2+} > K^+ \sim Na^+$; (4) the solvent-separated binding of the cations to the carboxylate groups of the chain is frequent, and its occurrence follows the approximate sequence $K^+ > Na^+ > Ca^{2+} > Mg^{2+}$ (contact-binding events as well as the binding of a cation to multiple carboxylate groups are very infrequent); and (5) the counter-ion atmosphere typically leads to a complete screening of the chain charge within 1.0–1.2 nm of the chain axis and, for most systems, to a charge reversal at about 1.5 nm (i.e. the effective chain charge becomes positive at this distance and as high in magnitude as one-quarter of the bare chain charge, before slowly decreasing to zero). These findings agree well (in a qualitative sense) with available experimental data and predictions from simple analytical models, and provide further insight concerning the nature of alginate–cation interactions in aqueous solution.

Keywords: computer simulation; molecular dynamics; alginates; polyguluronates; cation binding

1. Introduction

Polyuronates are (predominantly) polymers of uronic acids in (1 → 4)-linkage [1–5]. These polymers have diverse biological functions in plants, such as the preservation of the structure, texture and flexibility, as well as the prevention of dessication [6–12]. These functions are related to their ability to form gels [2–4,13–16], typically in the presence of divalent metal cations. The three most important natural derivatives of polyuronates are pectins [2–4,7–9,12,15,17–21], alginates [2–4,6,22] and glucuronans [23–25]. These polymers play a key role in food processing, biochemistry, biotechnology and environmental sciences [7,10,22,26–31].

Alginates [2–4,6,22] are linear copolymers of β-D-mannuronate (β-D-ManU) and α-L-guluronate (α-L-GulU; Figure 1) residues in (1 → 4)-linkage, predominantly alternating homogeneous segments of either type of residues and regular repeats of their dimer [32]. The relative amounts of the two acids and their distribution along the polymer chain vary widely depending on the natural source [6,22,33,34], and strongly influence the physico-chemical and biological properties of alginates [6,33–38]. They are present in large amounts in the extracellular medium of brown seaweeds (20–40% of the dry weight) and, for this reason, constitute the most abundant marine biopolymer.

An aqueous gel is formed when the polysaccharide chains associate through non-covalent interactions at the level of junction zones. These zones are separated by disordered segments consisting in general of only one chain. The framework of associated and disordered segments leaves large-sized cavities filled by water molecules. In the context of natural alginates, the size of the junction zones is typically limited by inhomogeneities in the polymer sequence. Homogeneous polyguluronate (pGulU) segments are believed to be the main contributors to junction zones [35,39–44] (although regular repeats of the α-[D-ManU-β(1 → 4)-L-GulU] dimer in (1 → 4)-linkage may also be involved [34,37,43,45]), while homogeneous polymannuronate segments (as well as segments with more heterogeneous sequences) show reduced propensities to chain–chain association. This size limitation of the junction zones prevents the formation of crystalline structures (precipitation) and, consequently, stabilises the polymer–water system in the gel state.

The gelation of polyuronates is generally induced by the addition of divalent metal cations (typically Ca^{2+}) at a pH close to neutrality. In this case, the leading

*Corresponding author. Email: phil@igc.phys.chem.ethz.ch

ISSN 0892-7022 print/ISSN 1029-0435 online

DOI: 10.1080/08927021003752853
http://www.informaworld.com

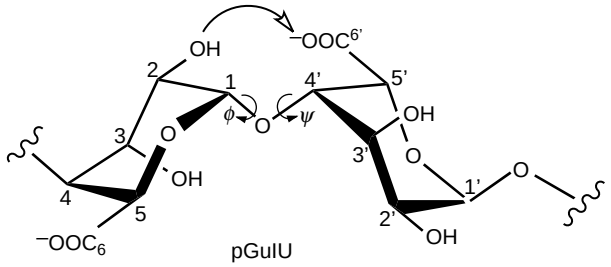

Figure 1. Structure of the (1 → 4)-linked α-L-GulU dimer, along with the atom labelling used in the present article (the primed residue is next to the unprimed residue towards the reducing end of the chain). The hydrogen bond $H_2 \rightarrow O_6'$ is also indicated by an arrow.

intermolecular interactions responsible for chain–chain association in the junction zones are ionic interactions between the negatively charged carboxylate groups and bridging divalent cations [2–4,42,46–48]. The most popular structural model for calcium-induced chain–chain association between pGulU segments in alginates is the so-called egg-box model [46,49,50], suggesting that pairs of segments in a 2_1-helical conformation are associated in an antiparallel fashion, leaving 'niches' for the calcium ions that are coordinated by carboxylate and hydroxyl groups of the two chains [46,49–54]. The egg-box model may not be the only model compatible with the available experimental data and has been questioned in a number of recent studies [35,45,51,53–58] (see [5] for an overview). However, irrespective of the details of the chain conformation and cation coordination mode, a primary dimerisation mechanism involving chain rigidification (regular helical structure) and tight ion binding (well-defined coordination sites) at junction zones associating (principally) homogeneous pGulU segments is generally accepted for the cation-induced gelation of alginates.

One important factor influencing the gelation of polyuronates in general (and of alginates in particular), as well as the properties of the resulting gels, is the nature and concentration of the cations present in solution. The experimental investigation of the influence of different counter-ions is not only interesting in terms of the elucidation of the gel formation mechanism, but also in terms of biological [59,60] (e.g. cell–cell adhesion) and environmental (e.g. concentration of heavy metals by plant roots or bacterial exopolysaccharides [61,62], adhesion of micro-organisms to surfaces and formation of biofilms [63,64]) issues, as well as practical applications (e.g. detoxification of heavy metal containing wastes [65–68], inhibition of the uptake of radioactive isotopes by the human body [69], design of wound dressing materials [70], biofouling of ultrafiltration or reverse-osmosis membranes [71,72], stabilisation of *in situ* drug release systems [73]).

The results of independent experimental studies concerning the cation binding selectivity of alginates are sometimes difficult to compare in detail, due to differences in the considered polymers (e.g. degree of polymerisation, GulU vs. ManU content and distribution), experimental conditions (e.g. soluble polymer vs. gel, detailed composition of the aqueous environment) and monitored properties (e.g. cation-exchange coefficients, gel strength, spectroscopic properties). However, considering simple (alkali and alkaline-earth) ions, the following main trends appear to be largely systematic:

(1) All (alkaline-earth) divalent metal cations (except for the Be^{2+} and Mg^{2+} cations [15,74–76]) are capable of promoting alginate gel formation. The selectivity towards these cations (as probed, for example, by cation-exchange coefficients, by the concentration of cations required to promote gel formation, or by the strength and permeability of the resulting gel) generally follows the sequence [14,26,27,69,75–91] $Ba^{2+} > Sr^{2+} > Ca^{2+} \gg Mg^{2+} > Be^{2+}$. This sequence appears to be dominated by the selectivity towards pGulU segments [69,79,80,88,89,92] (and inversions have been reported for ManU-rich alginates [89]). The same sequence appears to hold for both soluble (single-chain) and gel (junction zones) alginates, although the selectivity is weaker in the former case [82].

(2) The salts of alginates with monovalent (alkali) metal cations are typically water soluble (no gel formation in the absence of divalent cations). The selectivity towards these cations (as probed by ellipticity changes in circular dichroism measurements) appears to follow the sequence [93] $Li^+ < Na^+ < K^+ > Rb^+ > Cs^+$. Here also, the sequence appears to be dominated by the selectivity towards pGulU segments [93]. These experimental results suggest a peculiar binding mode for the Na^+ cations (which was tentatively interpreted as resulting from weak egg-box-like interchain interactions [93]). However, independent measurements of cation-exchange coefficients suggest a slightly enhanced binding of Na^+ compared to K^+ in soluble (single-chain) alginates [94] (i.e. an inversion between Na^+ and K^+ in the above sequence).

(3) Alginate chains evidence preferential affinity for divalent (alkaline-earth) over monovalent (alkali) metal cations. This selectivity is well known for the gels [46,86,95] (the divalent cations bound in junction zones cannot be displaced by monovalent cations, or only at very high relative concentration of monovalent ions [70,78,96–102]) and also appears to hold for soluble (single-chain) alginates [88,96,103]. Here again, the preferential affinity appears to be dominated by interactions with the pGulU segments [70,84,88,96,97,103,104].

The effect of different counter-ions (charge, size and concentration) on the gelation and resulting gel properties of polyuronates in general (and alginates in particular) can

be thought of as resulting from differences in polysaccharide–ion interactions in two distinct states: (1) free single chains in aqueous solution and (2) associated chains in junction zones. The present study exclusively focuses on the first state (the investigation of the second state will be the scope of a subsequent study).

In the free (unassociated) state, a polyuronate chain can be idealised as an infinite rod with regularly positioned negative charges, surrounded by (bound or aqueous) cations and neutralising (aqueous) anions. There exists a number of theoretical approaches to model such a rod-like polyanion surrounded by an aqueous counter-ion atmosphere. These include (in order of increasing complexity and expected accuracy): (1) analysis of the potential generated by the polyanion in vacuum and deduction of possible binding sites [54,105,106]; (2) analysis of the counter-ion distribution around the polyanion using simple solvation models based on continuum electrostatics along with different approximate treatments of interionic interactions, e.g. [107,108] linearised Poisson–Boltzmann [109,110], Poisson–Boltzmann [108,111–113] or Manning condensation [112–118] and extended [119–121] approaches; and (3) analysis of counter-ion trajectories (and corresponding calculated distributions) around the polyanion using Monte Carlo (MC), molecular dynamics (MD), stochastic dynamics (SD) or Brownian dynamics (BD) simulation techniques with an explicit representation of the counter-ions along with an implicit [122–124] (MC, SD and BD) or explicit [125] (MC and MD) representation of the solvent molecules. Although these approaches have been most commonly applied to the study of the deoxyribonucleic acid double helix, some have also been applied to polyuronates [5,54,105,106,126–131].

In a previous article [5], we applied an approach of the third type (explicit-solvent MD simulations) to investigate the binding of calcium ions (neutralising amount) to four types of homopolyuronate single chains at 300 K, starting from alternative regular two- and three-fold helical structures. In this work, the chains were made formally infinite by application of artificial periodicity along the chain axis (with octameric or nonameric repeat units). Two main observations made in these simulations were that: (1) the glycosidic linkages (and local helical parameters) showed an important flexibility (in time) and variability (along the chains), and regular helical structures only accounted for a limited fraction of the conformational ensembles populated at 300 K and (2) for all systems considered, the binding of the calcium counter-ions was essentially non-specific, with the formation of a dense counter-ion atmosphere around the chains (condensation), but no specific (tight-binding) interactions at well-defined coordination sites. Taken together, these observations suggested that if chain dimers are appropriately described by the egg-box model (or any other structural model with similar qualitative features), chain–chain association within junction zones in gels must be accompanied by substantial chain stiffening and a dramatic change in the ion-binding mode.

The goal of the present study is to investigate and compare the interaction of a set of monovalent (Na^+, K^+) and divalent (Mg^{2+}, Ca^{2+}) cations with single-chain pGulU (at 300 K and 1 bar) using explicit-solvent MD simulation. The approach employed is similar to that used in previous article [5], based on a (periodic) dodecameric pGulU chain in 2_1-helical conformation, and considers 14 possible combinations in terms of (neutralising) solution environments (single type of cation or simultaneous presence of two types of cation, either in the absence or presence of chloride anions).

2. Computational methods

2.1 MD simulation

All MD simulations were performed using the GROMOS96 program [132,133], together with the GROMOS 45A4 force field [134–139] (encompassing a recently reoptimised parameter set for hexopyranose-based carbohydrates [139–143], including uronates [5]) and the SPC water model [144]. The non-bonded interaction parameters for the ions were taken directly from the 45A4 force field except for K^+ (parameters optimised for the SPC model based on experimental single-ion hydration free energies assuming a value of $-1100\,\mathrm{kJ\,mol^{-1}}$ for the proton [145]; set *L* therein) and are provided as Supporting Information (Table S.I).

A total of 14 explicit-solvent simulations were carried out involving a single (periodic) pGulU chain in different counter-ion solutions (see below) at a temperature of 300 K and a pressure of 1 bar. The simulations were carried out under periodic boundary conditions based on cubic computational boxes (box edge *L*). The equations of motion were integrated using the leap-frog scheme [146], with a time step of 2 fs. The SHAKE algorithm [147] was applied to constrain all bond lengths with a relative geometric tolerance of 10^{-4}. The temperature was maintained close to its reference value (300 K) by weakly coupling the solute and solvent degrees of freedom separately to a heat bath [148], with a relaxation time of 0.1 ps. The pressure was also maintained close to its reference value (1 bar) by weakly coupling the particle coordinates and box dimensions (isotropic coordinate scaling) to a pressure bath [148], with a relaxation time of 0.5 ps and an isothermal compressibility of $0.4575 \times 10^{-3}\,\mathrm{kJ^{-1}\,mol\,nm^3}$ as appropriate for water [132]. The centre of mass motion was removed every 200 ps. Non-bonded interactions were computed using a twin-range scheme [125,132], with short- and long-range cut-off distances set to 0.8 and 1.4 nm, respectively, and a frequency of five time steps for the update of the short-range pairlist and intermediate-range interactions. A reaction-field correction [149,150] was applied to account for the

mean effect of omitted electrostatic interactions beyond the long-range cut-off distance, using a relative dielectric permittivity of 61 as appropriate for the SPC water model [151]. All simulations were carried out for a duration of 10 ns after an equilibration period of 1 ns, and coordinates were saved every 1 ps for subsequent analysis.

To avoid the presence of chain-end effects and the reduction of cooperativity associated with the simulation of finite (short) oligomers [106,126–131,152], the choice was made to simulate infinite chains by taking advantage of the periodic boundary conditions [5]. To this purpose, a polymer segment consisting of 12 residues within the computational box (with the chain axis aligned along the z-direction) was made infinite by linking the two terminal residues via a glycosidic bond across the periodic boundary (resulting in a formally cyclic topology [153]).

This approach is expected to account more appropriately for the cooperativity effects present within longer polymer chains and to entirely eliminate chain-end effects. However, one should be aware that the inclusion of an artificial periodic constraint with a repeat unit of 12 residues (along with an essentially fixed end-to-end vector for this 12-residue repeat, as imposed by the isotropic pressure coupling employed in the simulations and the limited compressibility of water) results in a restriction of the chain longitudinal and torsional flexibility [5]. The effect of the artificial longitudinal constraint is expected to be limited in view of the long persistence length (about 40 residues [5,154–158]) of pGulU. The effect of the torsional constraint is also expected to be limited by the consideration of a dodecameric periodic repeat (longer than in our previous article [5] and compatible with both regular two- and three-fold helices).

The initial structure for the simulations was chosen to be a regular 2_1-helix (six full turns per dodecameric repeat) with a turn angle per residue of 180° and a rise per residue $h_{\mathrm{ref}} = 0.427$ nm. The latter value was taken from the modelling studies by Braccini et al. [105] (based on MM3 relaxed-residue energy maps for the corresponding diuronic acids) and is close to the experimental value of 0.436 nm based on the fibre diffraction experiments by Atkins et al. [159–161] and Sikorski et al. [57]. This value is, however, lower than the value of 0.459 nm used in our previous article [5]. Initial coordinates for this chain configuration were generated using the program Insight II [162], assuming ideal $^4C_1$ ring geometries and using the reference ϕ and ψ glycosidic dihedral angle values ($\phi_{\mathrm{ref}} = 275.8°$ and $\psi_{\mathrm{ref}} = 84.7°$) reported by Braccini et al. [105]. The initial cubic box dimension L was set to $12\,h_{\mathrm{ref}}$. The computational boxes corresponding to the different systems were brought to overall neutrality by inclusion of counter-ions at random positions (see below) and filled to a water density of about 1 g cm^{-3}. After energy minimisation, equilibration was carried out by performing 0.2 ns MD simulation, increasing the temperature from 50 to 300 K in six successive steps followed by 0.8 ns at 300 K. The resulting configurations were then used for the production simulations.

The 14 simulations involved different solution environments in the form of overall neutralising sets of the different ions considered (Na^+, K^+, Mg^{2+}, Ca^{2+} and Cl^-) dissolved in about 4000 water molecules. The different combinations investigated (along with the resulting average box edges L, solution ionic strengths I and associated Debye screening lengths κ^{-1}) are summarised in Table 1. For the ease of reference, each simulation is labelled with a unique code referring to the solution environment it involves.

2.2 *Analysis of the trajectories*

The analysis of the trajectories was performed in terms of: (1) local helical conformation and intramolecular hydrogen bonding; (2) ion distribution and binding; (3) effective chain charge (charge of a cylindrical volume of given radius centred on the helix axis); and (4) chain (rotational, longitudinal and transverse) and ionic (three-dimensional, longitudinal and transverse) diffusion. The detailed procedures for these analyses are described elsewhere [5] and only the most important points are summarised below.

The local helical conformation at a glycosidic linkage was assessed by monitoring the corresponding turn angle. This angle is calculated as the dihedral angle between the 'reference vectors' of two successive residues, this vector being defined here as the projection of the vector connecting the midpoint of the C_2—C_3 bond to the midpoint of the C_5—O_5 bond onto the xy-plane (perpendicular to the helix axis). Values within ranges of ± 30° around 120, 180 or 240° were associated with local 3_1-, 2_1- or 3_2-helical conformations, respectively.

The intramolecular hydrogen bonding was only analysed in terms of the occurrences of the inter-residue $H_2 \rightarrow O_6'$ and $O_5 \leftarrow H_3'$ hydrogen bonds at the successive glycosidic linkages (where the primed residue is next to the unprimed residue towards the reducing end of the chain), since these two types of hydrogen bonds were the only ones found to be populated in regular polyuronate chains [5]. The presence of a hydrogen bond was defined by a maximal hydrogen–oxygen distance of 0.25 nm and a minimal oxygen–hydrogen–oxygen angle of 135°. A hydrogen bond between a hydroxyl and a carboxylate group was assumed to be present if the hydroxyl group formed a hydrogen bond with either (or both) of the carboxylate oxygen atoms.

The counter-ion distribution was analysed (for each ion type separately) in terms of the two-dimensional radial distribution function $g_{2D}(r)$ corresponding to the (minimum-image) distance r (in the xy-plane) between the helix axis and the ions of the given type. This function is defined in such a way that the integral of $L^{-2}2\pi r g_{2D}(r)$ over the

Table 1. Summary of the simulated systems.

System	Na^+	K^+	Mg^{2+}	Ca^{2+}	Cl^-	H_2O	L (nm)	I (mol kg^{-1})	I_{tot} (mol kg^{-1})	κ^{-1} (nm)	κ_{tot}^{-1} (nm)
Na	12	–	–	–	–	4147	5.05	0.08	0.16	1.08	0.76
K	–	12	–	–	–	4147	5.06	0.08	0.16	1.08	0.76
NaCl	24	–	–	–	12	4123	5.04	0.24	0.32	0.62	0.54
KCl	–	24	–	–	12	4123	5.05	0.24	0.32	0.62	0.54
NaKCl	12	12	–	–	12	4123	5.05	0.24	0.32	0.62	0.54
Mg	–	–	6	–	–	4153	5.05	0.16	0.24	0.76	0.62
Ca	–	–	–	6	–	4153	5.05	0.16	0.24	0.76	0.62
MgCl	–	–	12	–	12	4135	5.04	0.40	0.48	0.48	0.44
CaCl	–	–	–	12	12	4135	5.04	0.40	0.48	0.48	0.44
MgCaCl	–	–	6	6	12	4135	5.05	0.40	0.48	0.48	0.44
MgNaCl	12	–	6	–	12	4129	5.04	0.32	0.40	0.54	0.48
MgKCl	–	12	6	–	12	4129	5.05	0.32	0.40	0.54	0.48
CaNaCl	12	–	–	6	12	4129	5.05	0.32	0.40	0.54	0.48
CaKCl	–	12	–	6	12	4129	5.05	0.32	0.40	0.54	0.48

Notes: The reported entries for the 14 simulations are the simulation code, the types and numbers of counter-ions in the simulation box, the number of water molecules in the computational box, the average (cubic) box edge length (L) during the 10 ns simulations, the ionic strength (I, counter-ions only; I_{tot}, including the saccharide chain) and the Debye screening length (κ^{-1}, counter-ions only; κ_{tot}^{-1}, including the saccharide chain). The (root-mean-square) fluctuations of L are between 0.004 and 0.006 nm for all simulations. The ionic strength is calculated as $I = 1/2\sum b_i z_i^2$, where b_i is the solution molality of species i (mol solute per kg solvent) and z_i is the integer charge of the species (values including the saccharide consider individual monomeric units with an integer charge of -1). The Debye screening length is calculated as $\kappa^{-1} = CI^{-1/2}$ with $C = [(2N_A e^2 \rho_s)^{-1} \epsilon_o \epsilon_s k_B T]^{1/2}$, where N_A is Avogadro's number, e is the electron charge, ρ_s is the solvent density, ϵ_o is the permittivity of vacuum, ϵ_s is the relative dielectric permittivity of the solvent, k_B is Boltzmann's constant and T is the absolute temperature. Using the experimental values [174], $\rho_s = 997.048\,kg\,m^{-3}$ and $\epsilon_s = 78.36$ at $T = 300\,K$, one has $C = 0.305\,nm\,mol^{1/2}\,kg^{-1/2}$ (used for this table). Note that the use of appropriate values for the SPC water model, namely [151,175] $\rho_s = 994\,kg\,m^{-3}$ and $\epsilon_s = 61$, would lead to a slightly different value $C = 0.270\,nm\,mol^{1/2}\,kg^{-1/2}$. All simulations were carried out for 10 ns duration (after 1 ns equilibration) at 300 K and 1 bar.

entire distance range is equal to 1. The counter-ion distribution was also analysed in terms of the (three-dimensional) radial distribution function $g_{3D}(\rho)$ corresponding to the smallest (minimum-image) distance ρ between any of the two carboxylate oxygen atoms and the closest counter-ion. This function is defined in such a way that the integral of $L^{-3}4\pi\rho^2 g_{3D}(\rho)$ over the entire distance range is equal to 1. All radial distribution functions were computed with a bin width of 0.01 nm. In addition, cation-binding events were monitored for the 12 residues, by assigning two cut-off values ρ_t and ρ_l (with $\rho_t < \rho_l$) to the distance ρ. The condition $\rho \le \rho_t$ was associated with a tight-binding event (TB; contact ion pair), the condition $\rho_t < \rho \le \rho_l$ to a loose-binding event (LB; solvent-separated ion pair), while $\rho > \rho_l$ corresponded to the absence of ion binding. The values of ρ_t and ρ_l were chosen as the locations of the first and the second minima in $g_{3D}(\rho)$ for a given type of ion, i.e. the values of ρ_t were set to 0.30 (Na^+), 0.36 (K^+), 0.32 (Mg^{2+}) or 0.33 (Ca^{2+}) nm, while the corresponding values of ρ_l were set to 0.54 (Na^+), 0.61 (K^+), 0.52 (Mg^{2+}) or 0.57 (Ca^{2+}) nm. The binding (LB or TB) of the carboxylate group of a given residue to a cation that is simultaneously bound (LB or TB) to the carboxylate group of a different residue was referred to as a double-binding (DB; ion bridging) event. Two different types of DB events were further distinguished depending on whether they involved the carboxylate groups of two neighbour residues (DB_n) or of two second-neighbour residues (DB_s; i.e. separated by single residue along the chain). Finally, the counter-ion distributions were also visualised by superimposing successive trajectory frames (chain and counter-ions) onto the initial (equilibrated) chain configuration (rotational and translational fit based on the C_2, C_3, C_5 and O_5 atoms), and displaying the positions of all ions at successive 20 ps intervals.

The effective chain charge $Q(r)$ is defined as the net charge of a cylindrical volume of radius r centred on the helix axis (and of length corresponding to the simulated dodecameric unit). This quantity was evaluated as a function of r by summation of the charges contributed by all counter-ions (calculated via integration of the corresponding $g_{2D}(r)$ functions) with the boundary condition $Q(0) = -12\,e$ (chain charge).

Diffusion coefficients were calculated by monitoring the mean-square displacements $Q_{\mathbf{q}}(t)$ of various time-dependent quantities $\mathbf{q}(t)$, with averaging over all possible time origins. The corresponding diffusion coefficients $D_{\mathbf{q}}$ were calculated based on the Einstein relation, taking into account the dimensionality n (1, 2 or 3) of the quantity $\mathbf{q}$. In practice, $D_{\mathbf{q}}$ was estimated from the slope of a regression line fitting $Q_{\mathbf{q}}(t)$ over the interval from 0 to 3 ns where these functions were found to be approximately linear. The quantities $\mathbf{q}$ considered and the corresponding diffusion coefficients $D_{\mathbf{q}}$ were: (1) the chain orientation angle Θ (mean of the 'reference angles' of all residues, this angle being defined by the deviation of the above-defined reference vector relative to its orientation in the initial configuration; with $n = 1$), to evaluate the chain rotational diffusion constant D_Θ; (2) the z-coordinate of the chain centre (centre of geometry of the 'reference points' of all residues, this point being defined here as the centre of geometry of the ring atoms C_2, C_3, C_5 and O_5; with $n = 1$), to evaluate the chain longitudinal diffusion constant D_z;

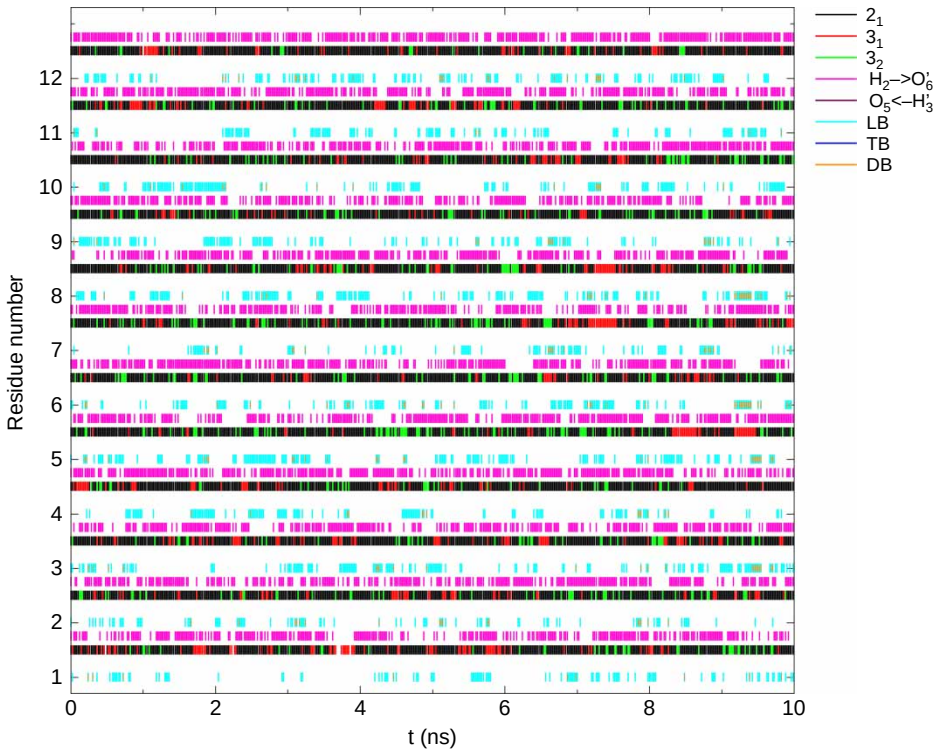

Figure 2. Time evolution of the local helical conformation, inter-residue hydrogen bonds and ion-binding events for the 12 glycosidic linkages in simulation Na (Table 1). The indicated events are the formation of a local 2_1-, 3_1- or 3_2-helical conformation, of $H_2 \rightarrow O_6'$ or $O_5 \leftarrow H_3'$ hydrogen bonds, of a solvent-separated (loose-binding, LB) ion pair, of a contact (tight-binding, TB) ion pair or of an ion pair (LB or TB) involving an ion also bound (LB or TB) to the carboxylate group of another residue (double binding, DB; smaller bars for the two involved carboxylate groups). The sampling period (individual bars) is 20 ps.

(3) the coordinate vector of the chain centre in the *xy*-plane (with $n = 2$), to evaluate the chain transverse diffusion constant D_{xy}; (4) the coordinate vector of a given counter-ion (with $n = 3$), to evaluate the three-dimensional diffusion constant $D_{i,r}$ for all counter-ions; (5) the *z*-coordinate of a given counter-ion (with $n = 1$), to evaluate longitudinal diffusion constants $D_{i,z}$ for all counter-ions; and (6) the coordinate vector of a given counter-ion in the *xy*-plane (with $n = 2$), to evaluate the transverse diffusion constants $D_{i,xy}$ for all counter-ions. While evaluating the corresponding time series $\mathbf{q}(t)$, care was taken to follow periodic coordinates as they diffused across different periods, without 'refolding' to the reference interval.

3. Results

3.1 Chain conformation and hydrogen bonding

The time evolution of the local helical conformation and inter-residue hydrogen bonding at the level of the 12 glycosidic linkages was found to be qualitatively very similar for all linkages and in all simulations. The results for simulation Na are displayed in Figure 2 as an illustrative example. The corresponding average occurrences are reported in Table 2 for the 14 simulations. In all cases, the number of full turns per dodecameric unit (sum of the turn angles of the 12 glycosidic linkages divided by 360°) remained exactly 6 throughout the entire simulation time (as appropriate for a chain conformation close to a 2_1-helix). The average rise per residue (average box edge

Table 2. Occurrences of local helical conformations and inter-residue hydrogen bonds for all simulations (Table 1).

System	2_1 (%)	3_1 (%)	3_2 (%)	$H_2 \rightarrow O_6'$ (%)	$O_5 \leftarrow H_3'$ (%)
Na	76.2	12.4	11.3	67.2	0.0
K	76.7	12.3	11.0	67.6	0.0
NaCl	76.6	12.2	11.0	67.0	0.0
KCl	76.3	12.4	11.1	66.7	0.0
NaKCl	78.1	11.3	10.5	68.0	0.0
Mg	76.4	12.0	11.4	67.3	0.0
Ca	75.2	12.9	11.9	66.9	0.0
MgCl	75.3	12.8	11.8	67.8	0.0
CaCl	77.3	11.8	10.7	68.9	0.0
MgCaCl	75.8	12.5	11.6	67.0	0.0
MgNaCl	76.2	12.6	11.1	66.7	0.0
MgKCl	76.9	12.3	10.7	68.2	0.0
CaNaCl	74.9	13.2	11.9	68.5	0.0
CaKCl	74.0	13.6	12.4	67.0	0.0

Notes: The occurrences are averaged over the 12 linkages and over the entire simulation time (10 ns). The indicated properties are the formation of a local 2_1-, 3_1- or 3_2-helical conformation and of $H_2 \rightarrow O_6'$ or $O_5 \leftarrow H_3'$ inter-residue hydrogen bonds.

length L divided by 12; Table 1) of about 0.420–0.422 nm is also the one appropriate for an ideal pGulU 2_1-helix (Section 2.1). Locally, the 2_1-helical conformation is also found to be predominant (74.0–78.1%), although alternative 3_1- (11.3–13.6%) and 3_2- (10.5–12.4%) conformations are also transiently observed. The $H_2 \rightarrow O_6'$ hydrogen bond is the only one found in the simulations (66.7–68.9%), while the $O_5 \leftarrow H_3'$ hydrogen bond is never observed. The occurences of local helical conformations and intramolecular hydrogen bonds found in the present simulations differ slightly (about 10% at most) from those reported in previous article [5] for pGulU. This is probably due to the consideration of dodecamers (rather than octamers) and to the slightly smaller value chosen here for the rise per residue (Section 2.1).

3.2 *Distribution of the ions around the chain*

The two-dimensional radial distribution functions $g_{2D}(r)$ of the different ions around the helix axis are displayed in Figures 3–5 for the 14 simulations. For the ease of comparison, a summary of the main features of these curves is also provided as Supporting Information (Table S.II).

The following general observations apply to all systems considered: (1) in the absence of Cl^- anions (simulations Na, K, Mg and Ca), the cation radial distributions are relatively narrow (narrow vs. broad referring here to the distance range spanned by the distribution) and tight (tight vs. loose referring here to the mean distance from the helix axis), presenting a single maximum at about 0.5–0.6 nm with a magnitude of about 6 (Na^+, K^+) or 8 (Mg^{2+}, Ca^{2+}), and essentially reaching zero (<0.25) beyond about 1.7 (Na^+, K^+) or 1.4 (Mg^{2+}, Ca^{2+}) nm; (2) in the presence of Cl^- anions along with a single cation type (simulations NaCl, KCl, MgCl and CaCl) or isovalent cation types (simulations NaKCl and MgCaCl), the cation distributions tend to be somewhat broader and looser (peak location usually shifted to a slightly higher distance, peak height decreased by a factor of about 1.8, appearance of a long-range tail in the distribution), compared to the corresponding simulations involving a single cation type in the absence of Cl^- (simulations Na, K, Mg and Ca); (3) in the presence of Cl^- ions along with cation types of different valences (simulations MgNaCl, MgKCl, CaNaCl and CaKCl), the distribution of the monovalent cation is significantly broadened and loosened (peak location shifted to about 0.8–0.9 nm, peak height decreased by a factor of about 2.2 in the presence of Mg^{2+} or 2.9 in the presence of Ca^{2+}, pronounced long-range tail in the distribution) compared to the corresponding simulation

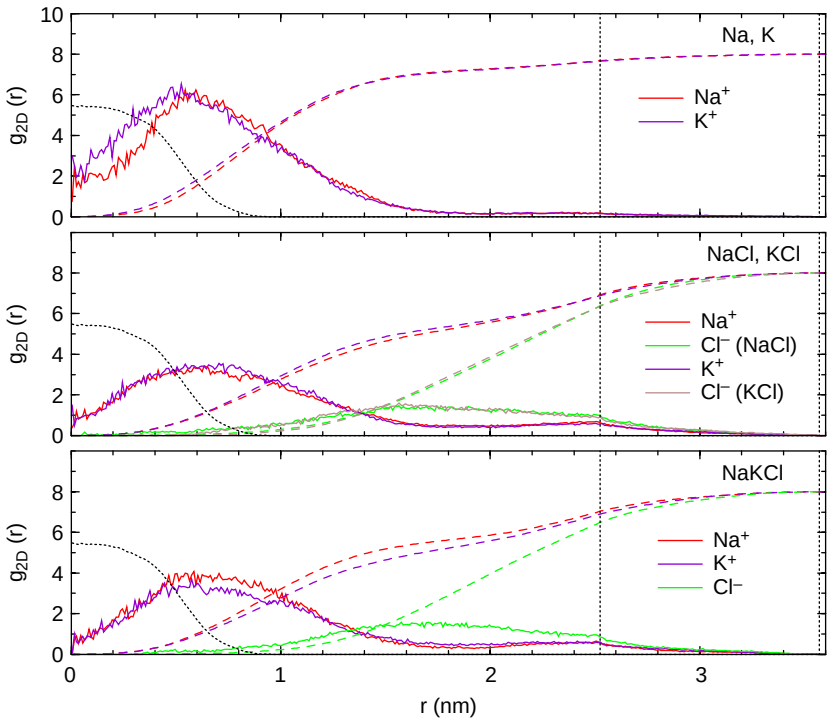

Figure 3. Two-dimensional radial distribution function $g_{2D}(r)$ for the coordinates of the counter-ions in the xy-plane relative to the helix axis for simulations Na, K, NaCl, KCl and NaKCl (Table 1). The functions are averaged over all ions of a given type in the system and calculated over the entire simulation time (10 ns) using a bin size of 0.01 nm. The cumulative integral of $L^{-2}2\pi r g_{2D}(r)$ is also displayed (amplified by a factor of eight for readability), as well as the corresponding distribution of all chain atoms (black dotted line; average over all simulations; scaled by a factor of five for readability).

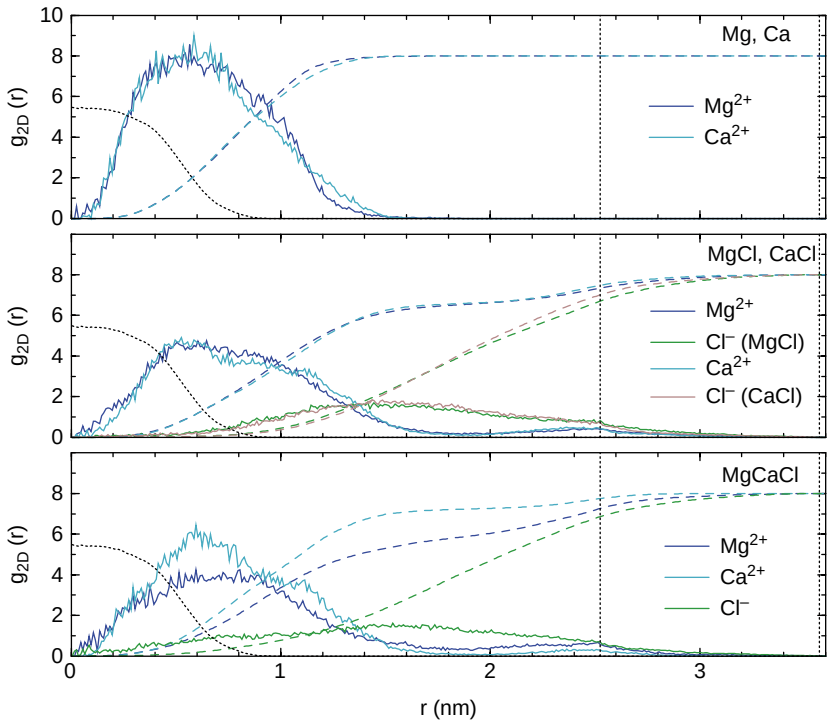

Figure 4. Two-dimensional radial distribution function $g_{2D}(r)$ for the coordinates of the counter-ions in the *xy*-plane relative to the helix axis for simulations Mg, Ca, MgCl, CaCl and MgCaCl (Table 1). The functions are averaged over all ions of a given type in the system and calculated over the entire simulation time (10 ns) using a bin size of 0.01 nm. The cumulative integral of $L^{-2}2\pi r g_{2D}(r)$ is also displayed (amplified by a factor of eight for readability), as well as the corresponding distribution of all chain atoms (black dotted line; average over all simulations; scaled by a factor of five for readability).

involving the monovalent ion alone (simulations Na and K), while the corresponding change in the distribution of the divalent cation (relative to simulations Mg and Ca) is much more limited; and (4) the distributions of the Cl^- anion (whenever present) are very broad and loose, presenting a single maximum at about 1.4–1.7 nm with a magnitude of about 1.4–1.7, and essentially vanishing (<0.25) below about 0.2–0.8 nm.

Qualitatively, these observations can be summarised as follows. When the chain charge is exactly neutralised by a single type of cation, divalent cations form a denser (narrower distribution) and tighter counter-ion atmosphere around the chain compared to monovalent cations. Upon addition of one equivalent of the chloride salt of the same ion or of an isovalent ion, the counter-ion atmosphere becomes slightly more diffuse (broader distribution) and less tight, as a result of the increased ionic strength (electrostatic screening) and of the competition between the chain and the chloride ions (predominantly distributed in the bulk region far away from the chain) for interactions with the cations. However, when one equivalent of the chloride salt of a monovalent cation is added to the chain neutralised by divalent cations (or, equivalently, the inverse process), the divalent cations preferentially interact with the chain (distribution similar to that observed for a chain neutralised by these sole cations) while the monovalent cations preferentially interact with the chloride ions (distribution significantly expanded compared to that observed for a chain neutralised by these sole cations). In other words, single pGulU chains in aqueous solution evidence a clear preferential affinity for divalent over monovalent cations when both types of ions are present in solution.

In addition to these general considerations, the detailed comparison of the different systems reveals the following differences between corresponding simulations involving a different type of monovalent (Na^+ or K^+) or divalent (Mg^{2+} or Ca^{2+}) cation. In the absence of divalent cations, the systems involving Na^+ or K^+ (simulations Na, K, NaCl, KCl and NaKCl) present very similar distributions for all types of ions (excepting a slightly tighter distribution for K^+ in simulation K compared to Na^+ in simulation Na in the immediate vicinity of the chain). The same applies to the systems involving Mg^{2+} or Ca^{2+} separately in the absence of monovalent cations (simulations Mg, Ca, MgCl and CaCl). However, when the two types of divalent cations are included simultaneously (simulation MgCaCl), the Ca^{2+} distribution is seen to be noticeably tighter compared to that of Mg^{2+} (simultaneously, the Cl^- distribution extends closer to the helix axis compared to all other systems). Finally, in the simulations involving cations of different valences

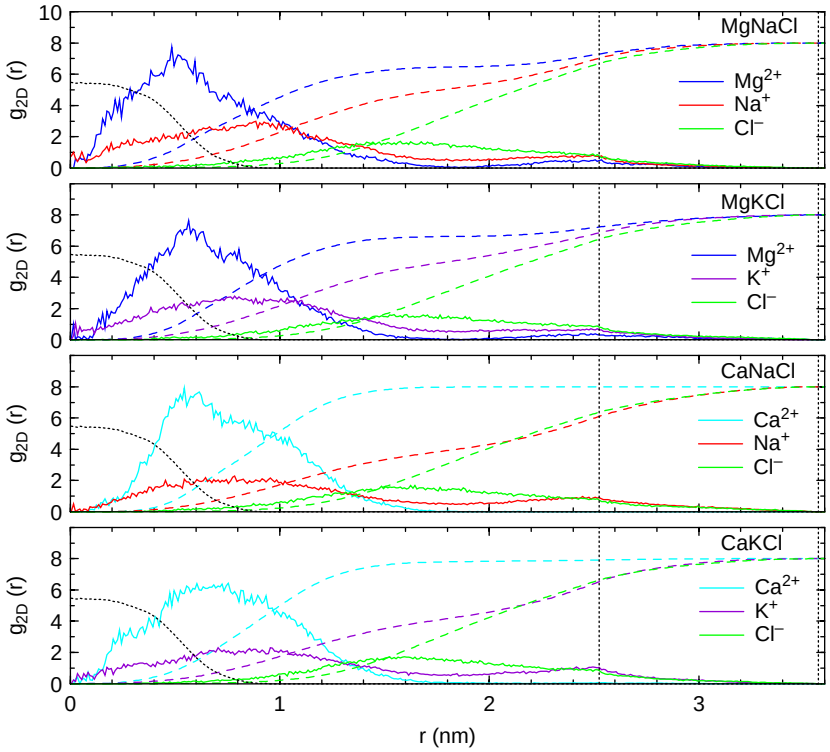

Figure 5. Two-dimensional radial distribution function $g_{2D}(r)$ for the coordinates of the counter-ions in the *xy*-plane relative to the helix axis for simulations MgNaCl, MgKCl, CaNaCl and CaKCl (Table 1). The functions are averaged over all ions of a given type in the system and calculated over the entire simulation time (10 ns) using a bin size of 0.01 nm. The cumulative integral of $L^{-2}2\pi r g_{2D}(r)$ is also displayed (amplified by a factor of eight for readability), as well as the corresponding distribution of all chain atoms (black dotted line; average over all simulations; scaled by a factor of five for readability).

(simulations MgNaCl, MgKCl, CaNaCl and CaKCl), a systematic difference is also seen between the systems involving the two different types of divalent cations. Irrespective of the monovalent cation considered, the Mg^{2+} distribution reaches closer to the helix axis (distance range 0.0–0.3 nm) compared to the Ca^{2+} distribution. However, in spite of this close-range difference, the Ca^{2+} distribution appears overall somewhat tighter (in contrast to Mg^{2+}, no long-distance tail is observed for Ca^{2+}) and the preferential exclusion of the monovalent cations is noticeably stronger for this divalent cation.

In summary, the density and tightness of the counter-ion atmosphere (in terms of an ion of a given type) appears to be correlated with the ion charge and size, resulting in the approximate ranking $Ca^{2+} > Mg^{2+} > K^{+} \sim Na^{+}$. Illustrative counter-ion distributions corresponding to simulations Na, NaCl, Ca, CaCl, NaKCl, MgCaCl, MgNaCl and CaNaCl are displayed graphically in Figure 6.

3.3 Ion binding to the chain

The statistics concerning the binding of the different cations to the carboxylate groups of the pGulU chain are reported in Table 3 for the 14 simulations.

The following general considerations apply to all systems considered: (1) the occurrence of ion-binding events (B), i.e. the average fraction of the simulation time where a carboxylate group binds a cation either tightly (TB; contact ion pair) or loosely (LB; solvent-separated ion pair), is significant (8.5–46.3%); (2) for the systems with one single cation type or two isovalent cation types (simulations Na, K, NaCl, KCl, NaKCl, Mg, Ca, MgCl, CaCl and MgCaCl), the binding events involving a monovalent cation are more frequent (27.4–46.3%) than those involving a divalent cation (23.1–27.4%); (3) for the systems involving cation types of different valences (simulations MgNaCl, MgKCl, CaNaCl and CaKCl), binding events involving a monovalent cation may be more frequent (Mg^{2+}) or less frequent (Ca^{2+}) than those involving a divalent cation; (4) the occurrence of tight-binding events (TB) is low (0.0–4.0%) and these events are noticeably less frequent for divalent (0.0–0.3%) compared to monovalent (0.3–4.0%) ions; (5) the occurrences of double-binding events (DB; ion bridging) are also low (0.6–11.9%), and these events are noticeably less frequent for divalent (0.6–3.9%) compared to monovalent (1.4–11.9%) ions; (6) the dominant contribution to DB events involves the simultaneous binding of an ion to two second-neighbour residues (DB_s) rather than

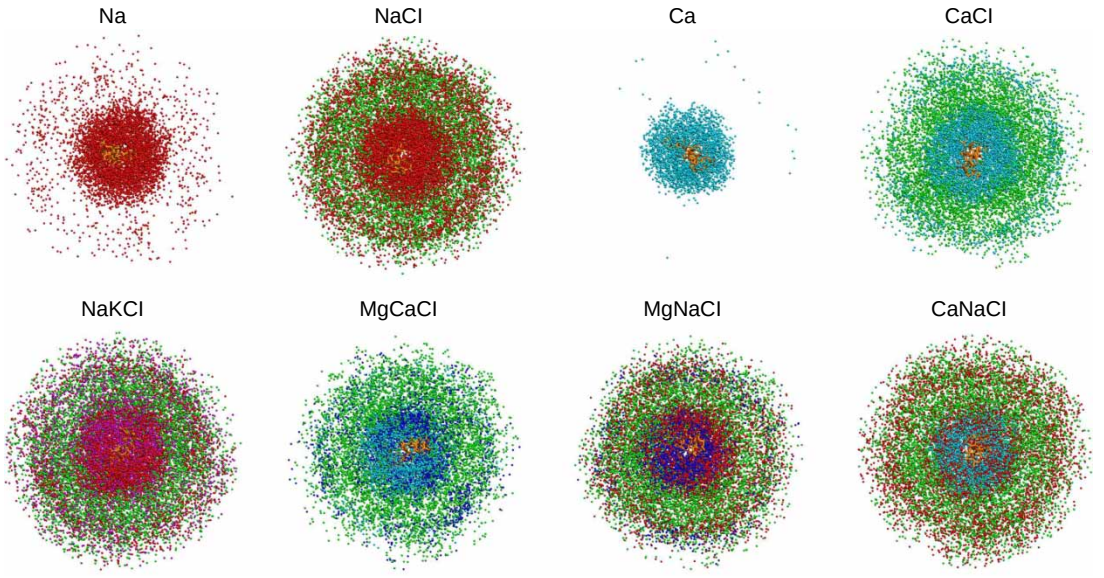

Figure 6. Positions of the counter-ions around the pGulU chain (top views), as sampled during eight simulations (Table 1). The ion coordinates correspond to successive configurations superimposed onto the initial one (rotational and translational fit based on the C_2, C_3, C_5 and O_5 atoms) over the entire (10 ns) simulations. The latter reference configuration is also displayed. Atom colouring: Na^+ (red), K^+ (magenta), Mg^{2+} (dark blue), Ca^{2+} (cyan) and Cl^- (green). The sampling period (interval between the ion positions displayed) is 20 ps.

two nearest-neighbour (DB_n) residues; and (7) the inclusion of Cl^- ions does not significantly affect the statistics of binding events (compared to the corresponding simulations without Cl^- ions). Note that triple-binding events were sometimes observed (their occurrence never exceeding 0.2%), while chloride-binding events were never observed.

Qualitatively, these observations can be summarised as follows (in the light of the corresponding general observations made in Section 3.2). The electrostatic attraction between the carboxylate groups and the cations is strong enough to promote the formation of a dense counter-ion atmosphere around the chain, along with a significant extent of non-specific solvent-separated counter-ion binding. However, this interaction is insufficient to induce the tight binding (contact ion pair) of the cations at specific sites, which would involve the partial desolvation of these ions. Furthermore, as discussed in previous work [5] (see figure 11 therein), due to the geometry of the chain (in the 2_1-helical conformation), the coordination of an ion by two carboxylate groups implies either a significant local distortion of the chain (DB_n event) or relatively long carboxylate-ion distances (DB_s event), so that such double-binding events are scarce (and only involve solvent-separated cation binding by the two carboxylate groups involved). These findings are in line with recent implicit-solvent modelling studies, suggesting that counter-ion binding to polyuronate single chains is (predominantly) a (non-specific) counter-ion condensation process [36,119–121]. The somewhat higher propensity of monovalent cations to be involved in LB, TB or DB events in the absence of divalent cations can be explained by their weaker solvation. In the presence of divalent ions, the inversion of this trend observed for Ca^{2+} probably results from the stronger preferential exclusion of the monovalent cations in this case (Section 3.2).

In addition to these general considerations, the detailed comparison of the different systems reveals the following differences between corresponding simulations involving a different monovalent (Na^+ or K^+) or divalent (Mg^{2+} or Ca^{2+}) cation. In the absence of divalent cations, the systems involving Na^+ or K^+ (simulations Na, K, NaCl, KCl and NaKCl) reveal a systematically higher occurrence of binding events of all types (B, LB, TB, DB_n, DB_s) for K^+ compared to Na^+ (e.g. increase by about 35–50% for B). Note that this systematic trend is not clearly correlated with a difference in the corresponding two-dimensional radial distribution functions (Section 3.2; with the possible exception of simulations Na vs. K). In contrast, the systems involving Mg^{2+} or Ca^{2+} separately in the absence of monovalent cations (simulations Mg, Ca, MgCl and CaCl) do not reveal a striking difference in terms of ion-binding properties. No differences are observed either in the corresponding radial distribution functions. However, when the two types of divalent cations are included simultaneously (simulation MgCaCl), a higher occurrence of binding events of all types is observed for Ca^{2+} compared to Mg^{2+} (e.g. occurrence higher by a factor of about 2 for B). In this case, the difference is clearly reflected in the corresponding radial

Table 3. Occurrence of cation-binding events of different types for all simulations (Table 1).

System	I	B (%)	LB (%)	TB (%)	DB (%)	DB_n (%)	DB_s (%)
Na	Na^+	27.4	26.8	0.6	3.9	0.5	3.4
K	K^+	41.7	38.2	3.5	11.9	2.4	9.6
NaCl	Na^+	33.2	32.7	0.5	6.3	0.4	5.9
KCl	K^+	46.3	42.4	4.0	10.9	2.8	8.1
NaKCl	Na^+	18.2	17.9	0.3	3.4	0.2	3.1
	K^+	24.5	22.8	1.7	7.0	1.3	5.7
	Cat	38.9	37.1	2.0	10.1	1.6	8.7
Mg	Mg^{2+}	27.4	27.4	0.0	2.1	0.2	1.9
Ca	Ca^{2+}	25.8	25.8	0.0	3.9	0.4	3.5
MgCl	Mg^{2+}	23.1	23.1	0.0	1.1	0.2	1.0
CaCl	Ca^{2+}	24.8	24.8	0.0	3.6	0.2	3.4
CaMgCl	Mg^{2+}	8.5	8.4	0.1	0.6	0.0	0.6
	Ca^{2+}	16.8	16.6	0.2	2.6	0.2	2.4
	Cat	24.7	24.5	0.3	3.2	0.2	3.0
MgNaCl	Mg^{2+}	13.1	13.1	0.0	2.7	0.3	2.4
	Na^+	15.1	14.6	0.4	3.0	0.6	2.5
	Cat	26.6	26.2	0.4	5.5	0.9	4.8
MgKCl	Mg^{2+}	15.0	15.0	0.0	1.2	0.0	1.2
	K^+	19.6	18.3	1.3	4.5	1.3	3.3
	Cat	33.0	31.7	1.3	5.7	1.3	4.5
CaNaCl	Ca^{2+}	19.4	19.1	0.3	2.1	0.4	1.7
	Na^+	10.8	10.4	0.3	1.4	0.2	1.1
	Cat	28.9	28.3	0.6	3.5	0.7	2.8
CaKCl	Ca^{2+}	18.0	18.0	0.0	2.6	0.1	2.4
	K^+	15.4	14.3	1.1	4.1	1.0	3.1
	Cat	31.5	30.6	1.1	6.6	1.1	5.5

Notes: The occurrences are averaged over the 12 carboxylate groups and over the entire simulation time (10 ns). The indicated properties are B (binding), solvent-separated (loose-binding, LB) ion pair, contact (tight-binding, TB) ion pair, double binding (DB, carboxylate group bound to an ion that is simultaneously bound to another carboxylate group), nearest-neighbour double binding (DB_n, DB event involving two nearest-neighbour residues), second-neighbour double binding (DB_s; DB event involving two second-neighbour residues). The notation 'Cat' represents any cation in the system irrespective of its identity.

distribution functions, where the Ca^{2+} distribution was found to be tighter than the Mg^{2+} distribution. Finally, in the simulations involving simultaneously ions with different valences (MgCaCl, MgKCl, CaNaCl and CaKCl), a systematic difference is also seen in terms of ion binding between the monovalent and the divalent cations. First, irrespective of the monovalent cation considered (Na^+ or K^+), the occurrences of binding events of all types are higher for Ca^{2+} compared to Mg^{2+}. Second, irrespective of the divalent cation considered, the corresponding occurrences are higher for K^+ compared to Na^+. Third, the binding of Mg^{2+} is enhanced by the presence of K^+ compared to Na^+, while the opposite is true for Ca^{2+}. Fourth, the binding of both Na^+ and K^+ are enhanced by the presence of Mg^{2+} compared to Ca^{2+}. Only the last trend could have been anticipated based on the observation of the corresponding radial distribution functions. In contrast, the first trend is somewhat unexpected considering that the close-range (0–3 nm) distribution of Mg^{2+} is higher than that of Ca^{2+}.

In summary, there appears to be no entirely systematic correlation between the trends observed in the distribution of the ions around the chain (Section 3.2) and the occurrence of ion-binding events (present section). Unless preferential affinity effects are involved (simulations involving ions of different valences simultaneously), the occurrence of binding events appears to be correlated with the ion charge and size, resulting in the approximate ranking $K^+ > Na^+ > Ca^{2+} > Mg^{2+}$. This ranking is also the one qualitatively expected in terms of increasing hydration strength of the cation. For example, the Na^+ cation is small, well hydrated, and usually classified as 'kosmotrope' [163–165] (meaning that Na^+ tends to promote water structuring around itself [166–169]). In contrast, the K^+ cation is larger, less well hydrated, and usually classified as 'chaotrope' [163,165] (meaning that K^+ exerts a moderate perturbation on water–water interactions in its vicinity [164,168,169]). In the context of the divalent cations, quantum-mechanical calculations [59,170–172] suggest that cation–carboxylate binding affinities are stronger in vacuum for Mg^{2+} compared to Ca^{2+}. However, this trend is inverted in aqueous solution [59] owing to the much higher salvation free energy of Mg^{2+} compared to Ca^{2+}.

3.4 Chain and ion diffusion

The chain rotational (D_Θ), longitudinal (D_z) and transverse (D_{xy}) diffusion constants as well as the ion three-dimensional ($D_{i,r}$), longitudinal ($D_{i,z}$) and transverse ($D_{i,xy}$) diffusion constants (the latter averaged over all ions of a given type) are reported in Table 4 for the 14 simulations.

Considering the chain, the rotational and longitudinal diffusion constants are found to be the highest in simulations Na, K, MgCl, CaCl and CaMgCl (the corresponding lateral diffusion constants do not evidence clear systematic trends). A more rapid chain diffusion suggests that these systems present either weaker cohesive forces between the chain and its counter-ion atmosphere or a weaker extent of hydration of the chain–atmosphere system (leading to a smaller 'effective' radius of the chain in solution). However, the observation of faster diffusion for these five specific systems does not obviously correlate with the trends observed previously in the two-dimensional radial distribution functions (Section 3.2) or ion-binding events (Section 3.3).

Considering the ions, the three-dimensional diffusion coefficients typically (but not entirely systematically) decrease in the order $Cl^- > K^+ > Na^+ > Ca^{2+} > Mg^{2+}$, which is also the trend observed experimentally for the free ions in solution (2.03, 1.96, 1.33, 0.79 and 0.71 $nm^2\,ns^{-1}$, respectively, as calculated from limiting molar conductivities of single ions [173] at 298.15 K; see eq. 6.7.23 in the quoted reference), a faster diffusion correlating with a weaker hydration

Table 4. Diffusion constants evaluated for different sets of degrees of freedom of the chain and of the counter-ions based on the 14 simulations (Table 1).

System	Chain/ion	D_Θ ($deg^2\,ns^{-1}$)	$D_{i,r}$ ($nm^2\,ns^{-1}$)	$D_z(D_{i,z})$ ($nm^2\,ns^{-1}$)	$D_{xy}(D_{i,xy})$ ($nm^2\,ns^{-1}$)
Na	Chain	8.93		1.22	0.08
	Na^+		1.54 (0.08)	1.63 (0.16)	1.49 (0.34)
K	Chain	12.27		0.89	0.12
	K^+		1.65 (0.04)	2.32 (0.17)	1.32 (0.19)
NaCl	Chain	1.53		0.22	0.24
	Na^+		2.69 (0.08)	3.42 (0.34)	2.33 (0.27)
	Cl^-		3.98 (0.14)	3.49 (0.30)	4.22 (0.81)
KCl	Chain	0.53		0.22	0.09
	K^+		1.98 (0.04)	2.44 (0.15)	1.75 (0.15)
	Cl^-		2.55 (0.05)	2.47 (0.26)	2.59 (0.29)
NaKCl	Chain	0.42		0.12	0.26
	Na^+		1.47 (0.03)	1.49 (0.10)	1.46 (0.16)
	K^+		2.08 (0.07)	1.89 (0.33)	2.18 (0.32)
	Cl^-		2.39 (0.07)	1.91 (0.18)	2.63 (0.39)
Mg	Chain	0.59		0.17	0.09
	Mg^{2+}		0.22 (0.01)	0.36 (0.04)	0.15 (0.02)
Ca	Chain	1.23		0.12	0.14
	Ca^{2+}		0.79 (0.07)	0.33 (0.04)	1.02 (0.38)
MgCl	Chain	2.28		0.32	0.04
	Mg^{2+}		1.36 (0.06)	0.89 (0.10)	1.59 (0.32)
	Cl^-		3.42 (0.16)	2.33 (0.19)	3.97 (0.96)
CaCl	Chain	5.42		0.36	0.06
	Ca^{2+}		2.47 (0.40)	0.84 (0.10)	3.29 (2.42)
	Cl^-		2.44 (0.08)	2.39 (0.23)	2.47 (0.41)
MgCaCl	Chain	3.60		1.06	0.19
	Mg^{2+}		2.01 (0.12)	1.89 (0.27)	2.06 (0.55)
	Ca^{2+}		1.08 (0.11)	0.67 (0.06)	1.28 (0.68)
	Cl^-		3.72 (0.15)	3.83 (0.53)	3.67 (0.52)
MgNaCl	Chain	0.61		0.36	0.19
	Mg^{2+}		0.51 (0.02)	0.81 (0.05)	0.36 (0.12)
	Na^+		1.36 (0.03)	1.46 (0.13)	1.31 (0.21)
	Cl^-		2.30 (0.05)	2.68 (0.20)	2.11 (0.30)
MgKCl	Chain	0.42		0.34	0.11
	Mg^{2+}		0.71 (0.03)	0.90 (0.19)	0.61 (0.19)
	K^+		2.49 (0.09)	3.17 (0.38)	2.15 (0.24)
	Cl^-		2.50 (0.06)	2.81 (0.23)	2.34 (0.32)
CaNaCl	Chain	1.16		0.13	0.21
	Ca^{2+}		0.49 (0.03)	0.66 (0.08)	0.40 (0.17)
	Na^+		1.82 (0.04)	1.53 (0.15)	1.97 (0.34)
	Cl^-		2.41 (0.07)	2.93 (0.24)	2.14 (0.29)
CaKCl	Chain	1.45		0.17	0.11
	Ca^{2+}		0.65 (0.03)	0.86 (0.08)	0.55 (0.19)
	K^+		2.61 (0.07)	1.80 (0.19)	3.02 (0.39)
	Cl^-		2.19 (0.04)	2.15 (0.18)	2.22 (0.21)

Notes: The diffusion coefficients D_q are calculated from a linear least-squares fit of the corresponding mean-square displacements $Q_q(t)$ over the time period from 0 to 3 ns, themselves calculated based on the entire simulation time (10 ns) considering all possible time origins. The chain diffusion is described in terms of the rotational (D_Θ), longitudinal (D_z) and transverse (D_{xy}) diffusion constants. The ionic diffusion is described in terms of the ionic three-dimensional ($D_{i,r}$), longitudinal ($D_{i,z}$) and transverse ($D_{i,xy}$) diffusion constants, averaged over all the counter-ions of a given type (the corresponding standard deviation divided by the square root of the number of ions is indicated between the parentheses as an error estimate).

strength. The main exception to this sequence is an inversion between Ca^{2+} and Mg^{2+} for the systems involving the two ions simultaneously or involving ions of different valences (simulations CaMgCl, MgNaCl, MgKCl, CaNaCl and CaKCl). This inversion can be related to the stronger interaction of Ca^{2+} with the chain in this case (Sections 3.2 and 3.3). Note also the other inversion between Na^+ and K^+ in the simulations involving the corresponding monovalent ion along with Cl^- anions (simulations NaCl and KCl). Since the comparison also reveals a significantly decreased mobility of Cl^- ions in the presence of K^+ (compared to Na^+), this inversion might result from a stronger interaction of K^+ with Cl^- (compared to Na^+ with Cl^-). Note finally that the longitudinal ionic diffusion coefficients tend to be higher than the transverse ones, although this trend is by no means systematic.

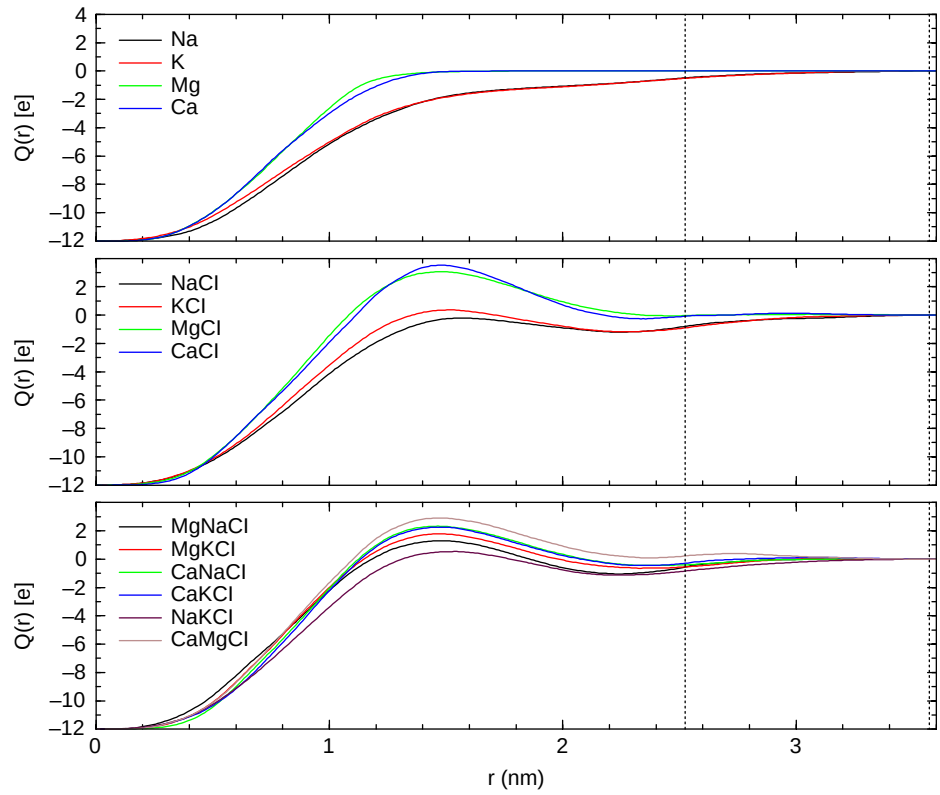

Figure 7. Effective chain charge $Q(r)$ as a function of the cylinder radius r for the 14 simulations (Table 1). This quantity represents the net charge of a cylindrical volume of radius r centred on the helix axis (and of length corresponding to the simulated dodecameric unit), and was calculated based on the two-dimensional radial distribution function $g_{2D}(r)$ of Figures 3–5. Vertical dashed lines indicate the approximate location of the nearest box wall and box corner.

3.5 *Effective chain charge*

The effective chain charge $Q(r)$ is displayed as a function of the cylinder radius r in Figure 7 for all simulations. The corresponding values at $r = 1.48$ and 2.33 nm (approximate locations of local maxima and minima, respectively, in the curves for systems involving more than one ion type) are provided as Supporting Information (Table S.III; along with the contributions of the different ions to the corresponding values). For the systems involving the chain neutralised by a single ion type in the absence of chloride ions (simulations Na, K, Mg and Ca), the effective charge increases monotonically from -12 (bare chain) to $0\,e$ (neutralised chain) over the entire distance range. The increase is steeper for the two simulations involving divalent cations compared to monovalent cations. In the former case, the quasi-complete ($>99\%$) neutralisation of the chain charge is reached at about 1.2 nm, while it is only reached at about 2.5 nm in the later case. This difference is expected on the basis of Debye–Hückel theory, the Debye screening lengths κ^{-1} corresponding to the two types of systems being 0.76 and 1.08 nm, respectively (Table 1). For the systems involving chloride ions, the effective charge curves are no longer monotonic and present a maximum at about 1.48 nm, followed by a minimum at about 2.33 nm, before reaching zero at longer distances. The effective charge at the maximum of the curve is positive (except for simulation NaCl), and particularly large for systems involving divalent cations (simulations MgCl, CaCl and MgCaCl; effective charge of about 2.9–3.5 e) and, to a lesser extent, for the systems involving cations of different valences (simulations MgNaCl, MgKCl, CaNaCl and CaKCl; effective charge of about 1.3–2.3 e). Furthermore, considering these systems, the simulations involving Ca^{2+} ions systematically present a higher positive charge at the maximum compared to the simulations involving Mg^{2+} (a similar difference is also observed in simulation MgCaCl, where Ca^{2+} provides the dominant positive contribution to this effective charge).

In summary, it appears that the charge screening afforded by the counter-ion atmosphere leads to a complete charge screening of the chain within about 1.0–2.5 nm of the chain axis (1.0–1.2 nm excluding simulations Na and K). Furthermore, in the presence of negative charges other than the sole chain charges (here, Cl^- anions), a charge reversal is actually observed close to 1.5 nm. This charge reversal is particularly strong in the presence of divalent (and especially Ca^{2+}) cations, where the magnitude of the (positive) effective chain charge at the maximum may be as high as about a quarter of that of the (negative) bare chain charge.

4. Conclusions

The goal of the present article was to investigate and compare the interaction of a set of monovalent (Na^+, K^+) and divalent (Mg^{2+}, Ca^{2+}) cations with single-chain pGulU (2_1-helical conformation) using explicit-solvent MD simulations, considering (overall neutral) systems involving one or two cation types, possibly along with chloride (Cl^-) anions. The main observations can be summarised as follows:

(1) The chain conformation, flexibility and intramolecular hydrogen bonding are insensitive to the ionic content of the surrounding solution.
(2) The binding of counter-ions to the chain appears to be largely non-specific, irrespective of the ionic content of the surrounding solution. The counter-ion atmosphere is almost entirely confined within a cylinder of high ionic density around the chain axis, with no well-defined binding sites. The carboxylate groups frequently (25–45%) bind cations, but nearly always remain in their second-solvation shells. Events of tight binding, as well as of multiple coordination, are scarce and of short durations [5].
(3) The density (spanned distance range) and tightness (closeness to the helix axis) of the distributions of specific cations within the counter-ion atmosphere follow the approximate order $Ca^{2+} > Mg^{2+} > K^+ \sim Na^+$. In particular, when both monovalent and divalent ions are present in solution, a clear preferential affinity for the latter ones is observed. Preferential affinity for Ca^{2+} over Mg^{2+} is also apparent, while K^+ and Na^+ behave very similarly.
(4) The frequency of ion-binding events for a specific cation (predominantly solvent-separated binding to a single carboxylate group) is not systematically related to the density and tightness of the corresponding ionic distribution within the counter-ion atmosphere, and follows the approximate order $K^+ > Na^+ > Ca^{2+} > Mg^{2+}$.
(5) The chain diffusion properties are not immediately correlated with the above properties (a faster diffusion is observed for simulations involving neutralising monovalent ions alone, or divalent ions in the presence of chloride ions). The ionic diffusion properties essentially follow the trends expected from bulk diffusion ($Cl^- > K^+ > Na^+ > Ca^{2+} > Mg^{2+}$; correlated with the hydration strength), and reveal a (non-systematic) trend towards faster longitudinal (as opposed to transverse) diffusion.
(6) The analysis of the effective chain charge reveals a nearly complete screening of the chain charge within 1.0–1.2 nm (excluding the simulations with a neutralising amount of monovalent cations alone) and a charge reversal close to 1.5 nm (excluding the simulations with a neutralising amount of cations alone; the effective chain charge at this distance being up to one-quarter of the magnitude of the bare chain charge).

The second observation is in line with the recent theoretical models suggesting that counter-ion binding to polyuronate single chains is (predominantly) a (non-specific) counter-ion condensation process [5,36,119–121]. The third observation is also qualitatively consistent with experimental results on the relative affinities of alkali and alkaline-earth cations for alginates (Section 1), with the possible exception of the close similarity between Na^+ and K^+ in the present simulations. Note, however, that experimentally observed differences [93,94] could be (at least in part) due to egg-box-like inter-chain interactions. Such interactions, if present, are obviously not accounted for in the present (single-chain) simulations. The preferential affinity for divalent over monovalent cations can easily be understood on the basis of simple arguments from Debye–Hückel or counter-ion condensation theory [36,119–121] (as previously discussed in the context of nucleic acids [122–124]). The difference between Mg^{2+} and Ca^{2+} is probably connected with more complex effects related to the hydration strength of the bare cation (as well as, possibly, cation–cation and cation–chloride interactions). The fourth observation suggests that (solvent-separated) cation binding to single-chain alginates is predominantly correlated with the hydration strength of the cation (in line with suggestions from previous theoretical work [59,170–172]). Finally, the sixth observation may have implications in the context of the kinetics of gel formation. Charge reversal effects [36,119–121] (also previously observed in the context of nucleic acids [122–124]) may significantly accelerate the speed of dimer formation by inducing a (temporary) Coulombic attraction between chain segments, i.e. permitting the approach of a less screened segment (negative apparent charge) with another more efficiently screened segment (positive apparent charge).

Taken together, the results of the present simulations provide a detailed (atomistic) picture of the interaction of ions with single-chain (pGulU segments in) alginates that is not directly accessible to experimental methods and is certainly more accurate than the description provided by simplified analytical theories. However, it should be stressed that a complete characterisation of the nature of alginate–cation interactions will require an analogous investigation in the context of associated chains (e.g. junction zones in gels). Such a study will be the scope of forthcoming articles.

Acknowledgements

The authors are grateful to Maria Reif for sharing her knowledge concerning ionic solvation properties and ion-solvation parameters.

References

[1] Y.S. Ovodov, *Structural chemistry of plant glycuronoglycans*, Pure Appl. Chem. 42 (1974), pp. 351–369.

[2] D.A. Rees and E.J. Welsh, *Secondary and tertiary structure of polysaccharides in solutions and gels*, Angew. Chem. Int. Ed. 16 (1977), pp. 214–224.

[3] D.A. Rees, *Polysaccharide shapes and their interactions – Some recent advances*, Pure Appl. Chem. 53 (1981), pp. 1–14.

[4] E.R. Morris, *Molecular interactions in polysaccharide gelation*, Br. Polym. J. 18 (1986), pp. 14–21.

[5] L. Perić, C.S. Pereira, S. Perez, and P.H. Hünenberger, *Conformation, dynamics and ion-binding properties of single-chain polyuronates: A molecular dynamics study*, Mol. Simul. 34 (2008), pp. 421–446.

[6] O. Smidsrød and K.I. Draget, *Chemistry and physical properties of alginates*, Carbohydr. Eur. 14 (1996), pp. 6–13.

[7] B.R. Thakur, R.K. Singh, and A.K. Handa, *Chemistry and uses of pectin – A review*, Crit. Rev. Food Sci. Nutr. 37 (1997), pp. 47–73.

[8] B.L. Ridley, M.A. O'Neill, and D. Mohnen, *Pectins: Structure, biosynthesis, and oligogalacturonide-related signaling*, Phytochemistry 57 (2001), pp. 929–967.

[9] W.G.T. Willats, L. McCartney, W. Mackie, and J.P. Knox, *Pectin: Cell biology and prospects for functional analysis*, Plant Mol. Biol. 47 (2001), pp. 9–27.

[10] H.P. Ramesh and R.N. Tharanathan, *Carbohydrates. The renewable raw materials of high biotechnological value*, Crit. Rev. Biotech. 23 (2003), pp. 149–173.

[11] Y. Fang, S. Al-Assaf, G.O. Philips, K. Nishinari, T. Funami, and P.A. Wiliams, *Participation of ions in promoting intermolecular associations of cell wall polysaccharides*, Struct. Chem. 20 (2009), pp. 317–324.

[12] A.G.J. Voragen, G.-J. Coenen, R.P. Verhoef, and H.A. Schols, *Pectin, a versatile polysaccharide present in plant cell walls*, Struct. Chem. 20 (2009), pp. 263–275.

[13] A.H. Clarke and S.B. Ross-Murphy, *Structural and mechanical properties of biopolymer gels*, Adv. Polym. Sci. 83 (1987), pp. 56–192.

[14] M. Rinaudo, *Non-covalent interactions in polysaccharide system*, Macromol. Biosci. 6 (2006), pp. 590–610.

[15] M. Rinaudo, *Polyelectrolyte properties of a plant and animal polysaccharide*, Struct. Chem. 20 (2009), pp. 277–289.

[16] P.A. Williams, *Molecular interactions of plant and algal polysaccharides*, Struct. Chem. 20 (2009), pp. 299–308.

[17] B. Boutherin, K. Mazeau, and I. Tvaroska, *Conformational statistics of pectin substances in solution by a Metropolis Monte Carlo*, Carbohydr. Polym. 31 (1997), pp. 1–12.

[18] S. Pérez, K. Mazeau, and C. Herve du Penhoat, *The three-dimensional structures of the pectic polysaccharides*, Plant Physiol. Biochem. 38 (2000), pp. 37–55.

[19] T. Duvetter, D.N. Sila, S. van Buggenhout, R. Jolie, A. van Loey, and M. Hendrickx, *Pectins in processed fruits and vegetables. Part I. Stability and catalytic activity of pectinases*, Compr. Rev. Food Sci. Food Saf. 8 (2009), pp. 75–85.

[20] D.N. Sila, S. van Buggenhout, T. Duvetter, I. Fraeye, A. de Roeck, A. van Loey, and M. Hendrickx, *Pectins in processed fruits and vegetables. Part II. Structure–function relationships*, Compr. Rev Food Sci. Food Saf. 8 (2009), pp. 86–104.

[21] S. van Buggenhout, D.N. Sila, T. Duvetter, A. van Loey, and M. Hendrickx, *Pectins in processed fruits and vegetables. Part III. Texture engineering*, Compr. Rev. Food Sci. Food Saf. 8 (2009), pp. 105–117.

[22] E. Onsoyen, *Commercial applications of alginates*, Carbohydr. Eur. 14 (1996), pp. 26–31.

[23] A. Heyraud, L. Dantas, J. Courtois, B. Courtois, W. Helbert, and H. Chanzy, *Crystallographic data on bacterial (1 → 4)-β-D-glucuronan*, Carbohydr. Res. 258 (1994), pp. 275–279.

[24] L. Dantas, A. Heyraud, B. Courtois, J. Courtois, and M. Milas, *Physicochemical properties of exogel exocellular β(1–4)-D-glucuronan from* Rhizobium meliloti *strain M5N1 C.S (NCIMB 40472)*, Carbohydr. Polym. 24 (1994), pp. 185–191.

[25] I. Braccini, A. Heyraud, and S. Pérez, *Three-dimensional features of the bacterial polysaccharide (1 → 4)-β-D-glucuronan: A molecular modeling study*, Biopolymers 45 (1998), pp. 165–175.

[26] D. Cozzi, P.G. Desideri, L. Lepri, and G. Ciantelli, *Alginic acid, a new thin layer material. Part I*, J. Chromatog. 35 (1968), pp. 390–404.

[27] D. Cozzi, P.G. Desideri, L. Lepri, and G. Ciantelli, *Thin-layer chromatography of metal ions on alginic acid. Part II*, J. Chromatog. 35 (1968), pp. 405–415.

[28] R.H. Walter, *Polysaccharide Association Structures in Food*, Marcel Dekker, New York, 1998.

[29] K.I. Draget, G. Skjåk-Braek, and O. Smidsrød, *Alginate based new materials*, Int. J. Biol. Macromol. 21 (1997), pp. 47–55.

[30] A.K. Anal and H. Singh, *Recent advances in microencapsulation of probiotics for industrial applications and target delivery*, Trends Food Sci. Tech. 18 (2007), pp. 240–251.

[31] M. Rinaudo, *Main properties and current applications of some polysaccharides as biomaterials*, Polym. Int. 57 (2008), pp. 397–430.

[32] D.A. Rees and J.W.B. Samuel, *The structure of alginic acid. Part VI. Minor features and structure variations*, J. Chem. Soc. C 22 (1967), pp. 2295–2298.

[33] A. Martinsen, G. Skjåk-Braek, and O. Smidsrød, *Alginate as immobilization material: I. Correlation between chemical and physical properties of alginate gel beads*, Biotechnol. Bioeng. 33 (1989), pp. 79–89.

[34] Y.A. Mørch, S. Holtan, I. Donati, B.L. Strand, and G. Skjåk-Braek, *Mechanical properties of C-5 epimerized alginates*, Biomacromolecules 9 (2008), pp. 2360–2368.

[35] Y. Yuguchi, H. Urakawa, K. Kajiwara, K.I. Draget, and B.T. Stokke, *Small-angle X-ray scattering and rheological characterization of alginate gels. 2. Time-resolved studies on ionotropic gels*, J. Mol. Struct. 554 (2000), pp. 21–34.

[36] C.K. Siew and P.A. Williams, *New insights into the mechanism of gelation of alginate and pectin: Charge annihilation and reversal mechanism*, Biomacromolecules 6 (2005), pp. 963–969.

[37] M. Dentini, G. Rinaldi, A. Barbetta, D. Risica, C. Anselmi, and G. Skjåk-Braek, *Ionic gel formation of a (pseudo)alginate characterized by an alternating MG sequence produced by epimerizing mannuronan with AlgE4*, Carbohydr. Polym. 67 (2007), pp. 465–473.

[38] M.A.K. Williams, A. Marshall, R.G. Haverkamp, and K.I. Draget, *Stretching single polysaccharide molecules using AFM: A potential method for the investigation of the intermolecular uronate distribution of alginate*, Food Hydrocolloids 22 (2008), pp. 18–23.

[39] O. Smidsrød, A. Haug, and B. Lian, *Properties of poly(1,4-hexuronates) in the gel state. II. Comparison of gels of different chemical compositions*, Acta Chem. Scand. 26 (1972), pp. 79–88.

[40] C.A. Steginsky, J.M. Beale, H.G. Floss, and R.M. Mayer, *Structural determination of alginic acid and the effect of calcium binding as determined by high-field NMR*, Carbohydr. Res. 225 (1992), pp. 11–26.

[41] Y. Qin, *Gel swelling properties of alginate fibers*, J. Appl. Polym. Sci. 91 (2004), pp. 1641–1645.

[42] N. Emmerichs, J. Wingender, H.-C. Flemming, and C. Mayer, *Interaction between alginates and manganese cations: Identification of preferred cation binding sites*, Int. J. Biol. Macromol. 34 (2004), pp. 73–79.

[43] K.I. Draget, G. Skjåk-Braek, and B.T. Stokke, *Similarities and differences between alginic acid gels and ionically crosslinked alginate gels*, Food Hydrocolloid 20 (2006), pp. 170–175.

[44] T.E. Jørgensen, M. Sletmoen, K.I. Draget, and B.T. Stokke, *Influence of oligoguluronates on alginate gelation, kinetics, and polymer organization*, Biomacromolecules 8 (2007), pp. 2388–2397.

[45] I. Donati, S. Holtan, Y.A. Morch, M. Borgogna, M. Dentini, and G. Skjåk-Braek, *New hypothesis on the role of alternating sequences in calcium-alginate gels*, Biomacromolecules 6 (2005), pp. 1031–1040.

[46] E.R. Morris, D.A. Rees, D. Thom, and J. Boyd, *Chiropractical and stoichiometric evidence of a specific, primary dimerisation*

process in alginate gelation, Carbohydr. Res. 66 (1978), pp. 145–154.
[47] J.-F. Thibault and M. Rinaudo, *Chain association of pectic molecules during calcium-induced gelation*, Biopolymers 25 (1986), pp. 455–468.
[48] C.W. Tibbits, A.J. MacDougall, and S.G. Ring, *Calcium binding and swelling behaviour of a high methoxyl pectin gel*, Carbohydr. Res. 310 (1998), pp. 101–107.
[49] G.T. Grant, E.R. Morris, D.A. Rees, P.J.C. Smith, and D. Thom, *Biological interactions between polysaccharides and divalent cations: The egg-box model*, FEBS Lett. 32 (1973), pp. 195–198.
[50] E.R. Morris, D.A. Powell, M.J. Gidley, and D.A. Rees, *Conformations and interactions of pectins I. Polymorphism between gel and solid states of calcium polygalacturonate*, J. Mol. Biol. 155 (1982), pp. 507–516.
[51] M.L. Dheu-Andries and S. Pérez, *Geometrical features of calcium–carbohydrate interactions*, Carbohydr. Res. 124 (1983), pp. 324–332.
[52] M.C. Jarvis and D.C. Apperley, *Chain conformation in concentrated pectic gels: Evidence from ^{13}C NMR*, Carbohydr. Res. 275 (1995), pp. 131–145.
[53] B.T. Stokke, K.I. Draget, O. Smisrod, Y. Yuguchi, H. Urakawa, and K. Kajiwara, *Small-angle X-ray scattering and rheological characterization of alginate gels. 1. Ca-alginate gels*, Macromolecules 33 (2000), pp. 1853–1863.
[54] I. Braccini and S. Pérez, *Molecular basis of Ca^{2+}-induced gelation in alginates and pectins: The egg-box model revisited*, Biomacromolecules 2 (2001), pp. 1089–1096.
[55] S. Arnott, W. Bian, R. Chandrasekaran, and B.R. Mains, *Lessons for today and tomorrow from yesterday – The structure of alginic acid*, Fibre Diffr. Rev. 9 (2000), pp. 44–51.
[56] L. Li, Y. Fang, R. Vreeker, and I. Appelquist, *Reexamining the egg-box model in calcium-alginate gels with X-ray diffraction*, Biomacromolecules 8 (2007), pp. 464–468.
[57] P. Sikorski, F. Mo, G. Skjåk-Braek, and B.T. Stokke, *Evidence for egg-box-compatible interactions in calcium-alginate gels from fiber X-ray diffraction*, Biomacromolecules 8 (2007), pp. 2098–2103.
[58] J.C. Cabrera, A. Boland, J. Messaien, P. Cambier, and P. van Custem, *Egg box conformation of oligogalacturonides: The time-dependent stabilization of the elicitor-active conformation increases its biological activity*, Glycobiology 18 (2008), pp. 473–482.
[59] T. Sulea and Z. Simon, *Calculation of ionic bridge contributions to homospecific interactions mediated by proteoglycans*, Internet Electron. J. Mol. Des. 1 (2002), pp. 59–63.
[60] O. Popescu, I. Checiu, P. Gherghel, and Z. Simon, *Quantitative and qualitative approach of glycan–glycan interactions in marine sponges*, Biochimie 85 (2003), pp. 181–188.
[61] P.H. Santschi, J.W. Murray, M. Baskaran, C.R. Benitez-Nelson, L.D. Guo, C.-C. Hung, C. Lamborg, S.B. Moran, U. Passow, and M. Roy-Barman, *Thorium speciation in seawater*, Marine Chem. 100 (2006), pp. 250–268.
[62] T.A. Davis, E.J.J. Kalis, J.P. Pinheiro, R.M. Town, and H.P. van Leeuwen, *Cd(II) speciation in alginate gels*, Environ. Sci. Technol. 42 (2008), pp. 7242–7247.
[63] D.C. Sobeck and M.J. Higgins, *Examination of three theories for mechanisms of cation-induced biofloculation*, Water Res. 36 (2002), pp. 527–538.
[64] M.A. Chappell and V.P. Evangelou, *Surface chemistry and function of microbial biofilms*, Adv. Agronom. 76 (2002), pp. 163–199.
[65] C. Hung, D. Tang, K.W. Warneken, and P.H. Santschi, *Distribution of carbohydrates, including uronic acid in estaurine waters of Galveston Bay*, Marine Chem. 73 (2001), pp. 305–318.
[66] F.T. Li, H. Yang, Y. Zhao, and R. Xu, *Novel modified pectin for heavy metal adsorption*, Chin. Chem. Lett. 18 (2007), pp. 325–328.
[67] A. Balaria and S. Schiewer, *Assessment of biosorption mechanism for Pb binding by citrus pectin*, Sep. Purif. Technol. 63 (2008), pp. 577–581.
[68] A. Maureira and B.L. Rivas, *Metal ions recovery with alginic acid coupled to ultrafiltration membrane*, Eur. Polym. J. 45 (2009), pp. 573–581.
[69] A. Haug and O. Smidsrød, *Strontium–calcium selectivity of alginates*, Nature 215 (1967), p. 757.
[70] Y. Qin, *Ion-exchange properties of alginate fibers*, Text. Res. J. 75 (2005), pp. 165–168.
[71] A.J. Abrahamse, C. Lipreau, and S.G.J. Heijman, *Removal of divalent cations reduces fouling of ultrafiltration membranes*, J. Membr. Sci. 323 (2008), pp. 153–158.
[72] X. Jin, X. Huang, and E.M.V. Hoek, *Role of specific ion interactions in seawater RO membrane fouling by alginic acid*, Environ. Sci. Technol. 43 (2009), pp. 3580–3587.
[73] H. Zimmermann, F. Ehrhart, D. Zimmermann, K Müller, A. Katsen-Globa, M. Behringer, P.J. Feilen, P. Gessner, G. Zimmermann, S.G. Shirley, M.M. Weber, J. Metze, and U. Zimmermann, *Hydrogel-based encapsulation of biological, functional tissues: Fundamentals, technologies and applications*, Appl. Phys. A 89 (2007), pp. 909–922.
[74] J.F. Thibault and M. Rinaudo, *Interactions of mono- and divalent counterions with alkali- and enzyme-deesterified pectins in salt-free solution*, Biopolymers 24 (1985), pp. 2131–2143.
[75] K.L. Chen, S.E. Mylon, and M. Elimelech, *Aggregation kinetics of alginate-coated hematite nanoparticles in monovalent and divalent electrolytes*, Environ. Sci. Technol. 40 (2006), pp. 1516–1523.
[76] K.L. Chen, S.E. Mylon, and M. Elimelech, *Enhanced aggregation of alginate-coated iron oxide (hematite) nanoparticles in the presence of calcium, strontium, and barium cations*, Langmuir 23 (2007), pp. 5920–5928.
[77] A. Haug, *The affinity of some divalent metals to different types of alginates*, Acta Chem. Scand. 15 (1961), pp. 1794–1795.
[78] A. Haug and O. Smidsrød, *The effect of divalent metals on the properties of alginate solutions. II. Comparison of different metal ions*, Acta Chem. Scand. 19 (1965), pp. 341–351.
[79] A. Haug and O. Smidsrød, *Fractionation of alginates by precipitation with calcium and magnesium ions*, Acta Chem. Scand. 19 (1965), pp. 1221–1226.
[80] O. Smidsrød and A. Haug, *Dependence upon uronic acid composition of some ion-exchange properties of alginates*, Acta Chem. Scand. 22 (1968), pp. 1989–1997.
[81] A. Haug and O. Smidsrød, *Selectivity of some anionic polymers for divalent metal ions*, Acta Chem. Scand. 24 (1970), pp. 843–854.
[82] O. Smidsrød and A. Haug, *Dependence upon the gel-sol state of the ion-exchange properties of alginate*, Acta Chem. Scand. 26 (1972), pp. 2063–2074.
[83] G.R. Seely and R.L. Hart, *The binding of alkali earth metal ions to alginates*, Macromolecules 7 (1974), pp. 706–710.
[84] R. Kohn, *Ion binding on polyuronates – Alginate and pectin*, Pure Appl. Chem. 3 (1975), pp. 371–397.
[85] D. Thom, G.T. Grant, E.R. Morris, and D.A. Rees, *Characterisation of cationic binding and gelation of polyuronates by circular dichroism*, Carbohydr. Res. 100 (1982), pp. 29–42.
[86] D.R. Crist, R.H. Crist, J.R. Martin, and J.R. Watson, *Ion exchange systems in proton–metal reactions with algal cell walls*, FEMS Microbiol. Rev. 14 (1994), pp. 309–314.
[87] Z.-Y. Wang, Q.-Z. Zhang, M. Konno, and S. Saito, *Sol-gel transition of alginate solution by the addition of various divalent cations: A rheological study*, Biopolymers 33 (1994), pp. 737–746.
[88] T.A. Davis, F. Llanes, B. Volesky, and A. Mucci, *Metal selectivity of* Sargassum *spp. and their alginates in relation to their α-L-guluronic acid content and conformation*, Environ. Sci. Technol. 37 (2004), pp. 261–267.
[89] Y.A. Mørch, I. Donati, B.L. Strand, and G. Skjåk-Braek, *Effect of Ca^{2+}, Ba^{2+}, and Sr^{2+} on alginate microbeads*, Biomacromolecules 7 (2006), pp. 1471–1480.
[90] H. Zimmermann, F. Wählisch, C. Baier, M. Westhoff, R. Reuss, D. Zimmermann, M. Behringer, F. Ehrhart, A. Katsen-Globa, C. Giese, U. Marx, V.L. Sukhorukov, J.A. Vasquez, P. Jakob, S.G. Shirley, and U. Zimmermann, *Physical and biological*

properties of barium cross-linked alginate membranes, Biomaterials 28 (2007), pp. 1327–1345.

[91] A.J. de Kerchove and M. Elimelech, *Calcium and magnesium cations enhance the adhesion of motile and nonmotile* Pseudomonas aerigunosa *on alginate films*, Langmuir 24 (2008), pp. 3392–3399.

[92] D. Lattner, H.-C. Flemming, and C. Mayer, *^{13}C-NMR study of the interaction of bacterial alginate with bivalent cations*, Int. J. Biol. Macromol. 33 (2003), pp. 81–88.

[93] R. Seale, E.R. Morris, and A. Rees, *Interactions of alginates with univalent cations*, Carbohydr. Res. 110 (1982), pp. 101–112.

[94] K.I. Draget, K. Steinsvag, E. Onsoyen, and O. Smidsrød, *Na- and K-alginate; effect on Ca^{2+}-gelation*, Carbohydr. Polym. 35 (1998), pp. 1–6.

[95] D.A. Rees, *Polysaccharide conformation in solutions and gels – Recent results on pectins*, Carbohydr. Polym. 2 (1982), pp. 254–263.

[96] O. Smidsrød and A. Haug, *The effect of divalent metals on the properties of alginate solutions. I. Calcium ions*, Acta Chem. Scand. 19 (1965), pp. 329–340.

[97] X. Wang and H.G. Spencer, *Calcium alginate gels: Formation and stability in the presence of an inert electrolyte*, Polymer 39 (1998), pp. 2759–2764.

[98] M.A. LeRoux, F. Guilak, and L.A. Setton, *Compressive and shear properties of alginate gel: Effects of sodium ions and alginate concentration*, J. Biomed. Mater. Res. 47 (1999), pp. 46–53.

[99] S.F. Simoni, T.N.P. Bosma, H. Harms, and A.J.B. Zehnder, *Bivalent cations increase both the subpopulation of adhering bacteria and their adhesion efficiency in sand columns*, Environ. Sci. Technol. 34 (2000), pp. 1011–1017.

[100] A.J. de Kerchove and M. Elimelech, *Structural growth and viscoelastic properties of adsorbed alginate layers in monovalent and divalents salt*, Macromolecules 39 (2006), pp. 6558–6564.

[101] A.J. de Kerchove and M. Elimelech, *Formation of polysaccharide gel layers in the presence of Ca^{2+} and K^{+} ions: Measurements and mechanisms*, Biomacromolecules 8 (2007), pp. 113–121.

[102] G. Chen and S.L. Walker, *Role of solution chemistry and ion valence on the adhesion kinetics of groundwater and marine bacteria*, Langmuir 23 (2007), pp. 7162–7169.

[103] R. Kohn, I. Furda, A. Haug, and O. Smidsrød, *Binding of calcium and potassium ions to some polyuronides and monouronates*, Acta Chem. Scand. 22 (1968), pp. 3098–3102.

[104] B. Thu, G. Skjåk-Braek, F. Micali, F. Vittur, and R. Rizzo, *The spatial distribution of calcium in alginate gel beads analyzed by synchrotron-radiation induced X-ray emission (SRIXE)*, Carbohydr. Res. 297 (1997), pp. 101–105.

[105] I. Braccini, R.P. Grasso, and S. Pérez, *Conformational and configurational features of acidic polysaccharides and their interactions with calcium ions: A molecular modeling investigation*, Carbohydr. Res. 317 (1999), pp. 119–130.

[106] T.D. Perry, IV, R.T. Cygan, and R. Mitchell, *Molecular models of alginic acid: Interactions with calcium ions and calcite surfaces*, Geochim. Cosmochim. Acta 70 (2006), pp. 3508–3532.

[107] C.F. Anderson and M.T. Record, Jr, *Ion distribution around DNA and other cylindrical polyons: Theoretical descriptions and physical implications*, Annu. Rev. Biophys. Biophys. Chem. 19 (1990), pp. 423–465.

[108] P. Grochowski and J. Trylska, *Continuum molecular electrostatics, salt effects, and counterion binding – A review of the Poisson–Boltzmann theory and its modifications*, Biopolymers 89 (2007), pp. 93–113.

[109] T.L. Hill, *Approximate calculation of the electrostatic free energy of nucleic acids and other cylindrical macromolecules*, Arch. Biochem. Biophys. 57 (1955), pp. 229–239.

[110] K. Wagner, E. Keyes, T.W. Kephart, and G. Edwards, *Analytical Debye–Hückel model for electrostatic potentials around dissolved DNA*, Biophys. J. 73 (1997), pp. 21–30.

[111] D.C. Rau and E. Charney, *Polarization of the ion atmosphere of a charged cylinder*, Biophys. Chem. 14 (1981), pp. 1–9.

[112] M. Le Bret and B. Zimm, *Distribution of counterion around a cylindrical polyelectrolite and Manning's condensation theory*, Biopolymers 23 (1984), pp. 287–312.

[113] D. Stigter, *Evaluation of the counterion condensation theory of polyelectrolytes*, Biophys. J. 69 (1995), pp. 380–388.

[114] G.S. Manning, *Limiting laws and counterion condensation in polyelectrolyte solutions. I. Colligative properties*, J. Chem. Phys. 51 (1969), pp. 924–933.

[115] G.S. Manning, *Limiting laws and counterion condensation in polyelectrolyte solutions. II. Self-diffusion of the small ions*, J. Chem. Phys. 51 (1969), pp. 934–938.

[116] G.S. Manning, *Limiting laws and counterion condensation in polyelectrolyte solutions. III. An analysis based on the Mayer ionic solution theory*, J. Chem. Phys. 51 (1969), pp. 3249–3252.

[117] G.S. Manning, *Limiting laws and counterion condensation in polyelectrolyte solutions. IV. The approach to the limit and the extraordinary stability of the charge fraction*, Biophys. Chem. 7 (1977), pp. 95–102.

[118] G.S. Manning, *Electrostatic free energies of spheres, cylinders, and planes in counterion condensation theory with some applications*, Macromolecules 40 (2007), pp. 8071–8081.

[119] I. Donati, A. Cesaro, and S. Paoletti, *Specific interactions versus counterion condensation. 1. Nongelling ions/polyuronate systems*, Biomacromolecules 7 (2006), pp. 281–287.

[120] I. Donati, J.C. Benegas, A. Cesaro, and S. Paoletti, *Specific interactions versus counterion condensation. 2. Theoretical treatment within the counterion condensation theory*, Biomacromolecules 7 (2006), pp. 1587–1596.

[121] I. Donati, J.C. Benegas, and S. Paoletti, *Polyelectrolyte study of the calcium-induced chain association of pectate*, Biomacromolecules 7 (2006), pp. 3439–3447.

[122] J.C.G. Montoro and J.L.F. Abascal, *Ionic distribution around simple DNA models. I. Cylindrically averaged properties*, J. Chem. Phys. 103 (1995), pp. 8273–8284.

[123] J.C.G. Montoro and J.L.F. Abascal, *Ionic distribution around simple B-DNA models. II. Deviations from cylindrical symmetry*, J. Chem. Phys. 109 (1998), pp. 6200–6210.

[124] J.L.F. Abascal and J.C.G. Montoro, *Ionic distribution around simple B-DNA models. III. The effect of ionic charge*, J. Chem. Phys. 114 (2001), pp. 4277–4284.

[125] W.F. van Gunsteren and H.J.C. Berendsen, *Computer simulation of molecular dynamics: Methodology, applications and perspectives in chemistry*, Angew. Chem. Int. Ed. 29 (1990), pp. 992–1023.

[126] B. Manunza, S. Deiana, and C. Gessa, *Molecular dynamics study of Ca-polygalacturonate clusters*, J. Mol. Struct. 368 (1996), pp. 27–29.

[127] B. Manunza, S. Delana, B. Pintore, and C. Gessa, *A molecular dynamics investigation on the occurrence of helices in polygalacturonic acid*, J. Mol. Struct. 419 (1997), pp. 169–172.

[128] B. Manunza, S. Deiana, M. Pintore, and C. Gessa, *Molecular dynamics study of polygalacturonic acid chains in aqueous solution*, Carbohydr. Res. 300 (1997), pp. 85–88.

[129] B. Manunza, S. Deiana, M. Pintore, and C. Gessa, *Interaction of Ca^{2+} and Na^{2+} ions with polygalacturonate chains: A molecular dynamics study*, Glycoconj. J. 15 (1998), pp. 297–300.

[130] R. Noto, V. Martorana, D. Bulone, and P.L. San Biagio, *Role of charges and solvent on the conformational properties of poly(galacturonic acid) chains: A molecular dynamics study*, Biomacromolecules 6 (2005), pp. 2555–2562.

[131] M. Eriksson, T.K. Lindhorst, and B. Hartke, *Differential effects of oligosaccharides on the hydration of simple cations*, J. Chem. Phys. 128 (2008), pp. 105105/1–105105/10.

[132] W.F. van Gunsteren, S.R. Billeter, A.A. Eising, P.H. Hünenberger, P. Krüger, A.E. Mark, W.R.P. Scott, and I.G. Tironi, *Biomolecular Simulation: The GROMOS96 Manual and User Guide*, Verlag der Fachvereine, Zürich, Switzerland, 1996.

[133] W.R.P. Scott, P.H. Hünenberger, I.G. Tironi, A.E. Mark, S.R. Billeter, J. Fennen, A.E. Torda, T. Huber, P. Krüger, and W.F. van Gunsteren, *The GROMOS biomolecular simulation program package*, J. Phys. Chem. A 103 (1999), pp. 3596–3607.

[134] L.D. Schuler and W.F. van Gunsteren, *On the choice of dihedral angle potential energy functions for n-alkanes*, Mol. Simul. 25 (2000), pp. 301–319.

[135] L.D. Schuler, X. Daura, and W.F. van Gunsteren, *An improved GROMOS96 force field for aliphatic hydrocarbons in the condensed phase*, J. Comput. Chem. 22 (2001), pp. 1205–1218.

[136] I. Chandrasekhar, M.A. Kastenholz, R.D. Lins, C. Oostenbrink, L.D. Schüler, D.P. Tieleman, and W.F. van Gunsteren, *A consistent potential energy parameter set for lipids: Dipalmitoylphosphatidylcholine as a benchmark of the GROMOS9645A3 force field*, Eur. Biophys. J. 32 (2003), pp. 67–77.

[137] T.A. Soares, P.H. Hünenberger, M.A. Kastenholz, V. Kräutler, T. Lenz, R.D. Lins, C. Oostenbrink, and W.F. van Gunsteren, *An improved nucleic-acid parameter set for the GROMOS force field*, J. Comput. Chem. 26 (2005), pp. 725–737.

[138] U. Börjesson and P.H. Hünenberger, *pH-Dependent stability of a decalysine alpha-helix studied by explicit-solvent molecular dynamics simulations at constant pH*, J. Phys. Chem. B 108 (2004), pp. 13551–13559.

[139] R.D. Lins and P.H. Hünenberger, *A new GROMOS force field for hexopyranose-based carbohydrates*, J. Comput. Chem. 26 (2005), pp. 1400–1412.

[140] C.S. Pereira, D. Kony, R. Baron, M. Müller, W.F. van Gunsteren, and P.H. Hünenberger, *Conformational and dynamical properties of disaccharides in water: A molecular dynamics study*, Biophys. J. 90 (2006), pp. 4337–4344.

[141] V. Kräutler, M. Müller, and P.H. Hünenberger, *Conformation, dynamics, solvation and relative stabilities of selected β-hexopyranoses in water: A molecular dynamics study with the GROMOS 45A4 force field*, Carbohydr. Res. 342 (2007), pp. 2097–2124.

[142] H.S. Hansen and P.H. Hünenberger, *Using the local elevation method to construct optimized umbrella sampling potentials: Calculation of the relative free energies and interconversion barriers of glucopyranose ring conformers in water*, J. Comput. Chem. 31 (2010), pp. 1–23.

[143] L. Perić-Hassler, H.S. Hansen, R. Baron, and P.H. Hünenberger, *Conformational properties of glucose-based disaccharides using molecular dynamics simulations with local elevation umbrella sampling*, Carbohydr. Res. (2010), submitted.

[144] H.J.C. Berendsen, J.P.M. Postma, W.F. van Gunsteren, and J. Hermans, *Interaction models for water in relation to protein hydration*, in *Intermolecular Forces*, B. Pullman, ed., Reidel, Dordrecht, The Netherlands, 1981, pp. 331–342.

[145] M.M. Reif and P.H. Hünenberger, *Computation of methodology-independent single-ion solvation properties from molecular simulations. IV. Optimized Lennard-Jones interaction parameter sets for the alkali and halide ions in water*, J. Chem. Phys. (2010), submitted.

[146] R.W. Hockney, *The potential calculation and some applications*, Methods Comput. Phys. 9 (1970), pp. 136–211.

[147] J.-P. Ryckaert, G. Ciccotti, and H.J.C. Berendsen, *Numerical integration of the Cartesian equations of motion of a system with constraints: Molecular dynamics of n-alkanes*, J. Comput. Phys. 23 (1977), pp. 327–341.

[148] H.J.C. Berendsen, J.P.M. Postma, W.F. van Gunsteren, A. Di Nola, and J.R. Haak, *Molecular dynamics with coupling to an external bath*, J. Chem. Phys. 81 (1984), pp. 3684–3690.

[149] J.A. Barker and R.O. Watts, *Monte Carlo studies of the dielectric properties of water-like models*, Mol. Phys. 26 (1973), pp. 789–792.

[150] I.G. Tironi, R. Sperb, P.E. Smith, and W.F. van Gunsteren, *A generalized reaction field method for molecular dynamics simulations*, J. Chem. Phys. 102 (1995), pp. 5451–5459.

[151] T.N. Heinz, W.F. van Gunsteren, and P.H. Hünenberger, *Comparison of four methods to compute the dielectric permittivity of liquids from molecular dynamics simulations*, J. Chem. Phys. 115 (2001), pp. 1125–1136.

[152] V.L. Larwood, B.J. Howlin, and G.A. Webb, *Solvation effects on the conformational behaviour of gellan and calcium ion binding to gellan double helices*, J. Mol. Model. 2 (1996), pp. 175–182.

[153] D. Kony, W. Damm, S. Stoll, W.F. van Gunsteren, and P.H. Hünenberger, *Explicit-solvent molecular dynamics simulations of the polysaccharide schizophyllan in water*, Biophys. J. 93 (2007), pp. 442–455.

[154] I.G. Plashchina, M.G. Semenova, E.E. Braudo, and V.B. Tolstoguzov, *Structural studies of the solutions of anionic polysaccharides IV. Study of pectin solutions by light-scattering*, Carbohydr. Polym. 5 (1985), pp. 159–179.

[155] S. Cros, C. Garnier, M.A.V. Axelos, A. Imberty, and S. Pérez, *Solution conformations of pectin polysaccharides: Determination of chain characteristics by small angle neutron scattering, viscometry, and molecular modeling*, Biopolymers 39 (1996), pp. 339–352.

[156] F. Avaltroni, M. Seijo, S. Ulrich, S. Stoll, and K.J. Wilkinson, *Conformational changes and aggregation of alginic acid as determined by fluorescence correlation spectroscopy*, Biomacromolecules 8 (2007), pp. 106–112.

[157] B.E. Christensen, G. Skjåk-Braek, and O. Smidsrød, *Comment on 'conformational changes and aggregation of alginic acid as determined by fluorescence correlation spectroscopy'*, Biomacromolecules 8 (2007), p. 3279.

[158] F. Avaltroni, M. Seijo, S. Ulrich, S. Stoll, and K.J. Wilkinson, *Reply to comment on 'conformational changes and aggregation of alginic acid as determined by fluorescence correlation spectroscopy'*, Biomacromolecules 8 (2007), p. 3280.

[159] E.D.T. Atkins, W. Mackie, and E.E. Smolko, *Crystalline structures of alginic acids*, Nature 225 (1970), pp. 626–628.

[160] E.D.T. Atkins, W. Mackie, K.D. Parker, and E.E. Smolko, *Crystalline structures of poly-D-mannuronic and poly-L-guluronic acids*, Polym. Lett. 9 (1971), pp. 311–316.

[161] E.D.T. Atkins, H.H. Nieduszynski, W. Mackie, K.D. Parker, and E.E. Smolko, *Structural components of alginic acid. II. The crystalline structure of poly-α-L-guluronic acid. Results of X-ray diffraction and polarized infrared studies*, Biopolymers 12 (1973), pp. 1879–1887.

[162] Insight II *Molecular Modelling Package*, Molecular Simulations Inc. 2000.

[163] R.W. Gurney, *Ionic Processes in Solution*, McGraw-Hill, New York, 1953.

[164] K.D. Collins, *Charge density-dependent strength of hydration and biological structure*, Biophys. J. 72 (1997), pp. 65–76.

[165] Y. Marcus, *Effects of ions on the structure of water: Structure making and breaking*, Chem. Rev. 109 (2009), pp. 1346–1370.

[166] M.H. Abraham, J. Liszi, and E. Papp, *Calculations on ionic solvation. Part 6. Structure-making and structure-breaking effects of alkali halide ions from electrostatic entropies of solvation. Correlation with viscosity B-coefficients, nuclear magnetic resonance B′-coefficients and partial molal volumes*, J. Chem. Soc. Faraday Trans. 1 78 (1982), pp. 197–211.

[167] B. Hribar, N.T. Southall, V. Vlachi, and K.A. Dill, *How ions affect the structure of water*, J. Am. Chem. Soc. 124 (2002), pp. 12302–12311.

[168] R. Mancinelli, A. Botti, F. Bruni, M.A. Ricci, and A.K. Soper, *Perturbation of water structure due to monovalent ions in solution*, Phys. Chem. Chem. Phys. 9 (2007), pp. 2959–2967.

[169] S.S. Azam, T.S. Hofer, B.R. Randolf, and B.M. Rode, *Hydration of sodium(I) and potassium(I) revisited: A comparative QM/MM and QMCF MD simulation study of weakly hydrated ions*, J. Phys. Chem. A 113 (2009), pp. 1827–1834.

[170] V. Careja, M. Banda, L. Saity, C. Bologa, M. Mracec, and Z. Simon, *Possible saline bonds in peptidoglycan interactions. Steric considerations and sulfate and carbonate solubilities*, Proc. Rom. Acad. Ser. B 3 (2000), pp. 187–190.

[171] V. Careja, M. Mracec, L. Sayti, E. Sisu, R. Tudose, and Z. Simon, *Comparative study of some ionic bridges implying calcium and magnesium cations by computational methods*, Rev. Roum. Chim. 51 (2006), pp. 379–383.

[172] V. Careja, S. Muntean, M. Mracec, L. Sayti, and Z. Simon, *Molecular modeling of some calcium and magnesium ionic bridges*, Int. J. Quant. Chem. 107 (2007), pp. 1714–1718.

[173] W.R. Fawcett, *Liquids, Solutions and Interfaces*, Oxford University, Oxford, 2004.

[174] D.R. Lide, *CRC Handbook of Chemistry and Physics* (Internet version), 88th ed., CRC Press, Boca Raton, FL, 2008.

[175] A. Glättli, X. Daura, and W.F. van Gunsteren, *Derivation of an improved simple point charge model for liquid water: SPC/A and SPC/L*, J. Chem. Phys. 116 (2002), pp. 9811–9828.